Chinese Chemical Letters 34 (2023) 108075

Contents lists available at ScienceDirect

Chinese Chemical Letters

journal homepage: www.elsevier.com/locate/cclet

Review on electrochemical carbon dioxide capture and transformation with bipolar membranes

Jinyun Xu[a,1,*], Guoqiang Zhong[a,1], Minjing Li[a], Di Zhao[a], Yu Sun[a], Xudong Hu[b], Jiefang Sun[c], Xiaoyun Li[d], Wenju Zhu[a], Ming Li[a], Ziqi Zhang[a], Yu Zhang[a], Liping Zhao[a], Chunming Zheng[a,*], Xiaohong Sun[b,*]

[a] School of Chemical Engineering, Tianjin Key Laboratory of Green Chemical Technology and Process Engineering, State Key Laboratory of Separation Membrane and Membrane Processes, Tiangong University, Tianjin 300387, China
[b] School of Materials Science and Engineering, Key Laboratory of Advanced Ceramics and Machining Technology, Ministry of Education, Tianjin University, Tianjin 300072, China
[c] Beijing Key Laboratory of Diagnostic and Traceability Technologies for Food poisoning, Beijing Center for Disease Prevention and Control, Beijing 100013, China
[d] Advanced Materials Research Laboratory, CNOOC Tianjin Chemical Research and Design Institute, Tianjin 300131, China

ARTICLE INFO

Article history:
Received 19 August 2022
Revised 16 September 2022
Accepted 14 December 2022
Available online 16 December 2022

Keywords:
Bipolar membranes
Carbon dioxide
Electrochemical capture
Transformation
CO_2 reduction
Electrodialysis devices
Water dissociation

ABSTRACT

Anthropogenic carbon dioxide (CO_2) emission from the combustion of fossil fuels aggravates the global greenhouse effect. The implementation of CO_2 capture and transformation technologies have recently received great attention for providing a pathway in dealing with global climate change. Among these technologies, electrochemical CO_2 capture technology has attracted wide attention because of its environmental friendliness and flexible operating processes. Bipolar membranes (BPMs) are considered as one of the key components in electrochemical devices, especially for electrochemical CO_2 reduction and electrodialysis devices. BPMs create an alkaline environment for CO_2 capture and a stable pH environment for electrocatalysis on a single electrode. The key to CO_2 capture in these devices is to understand the water dissociation mechanism occurring in BPMs, which could be used for optimizing the operating conditions for CO_2 capture and transformation. In this paper, the references and technologies of electrochemical CO_2 capture based on BPMs are reviewed in detail, thus the challenges and opportunities are also discussed for the development of more efficient, sustainable and practical CO_2 capture and transformation based on BPMs.

1. Introduction

In the past decades, with the increase of population and the extensive use of fossil fuels, CO_2 emissions have caused severe greenhouse effect [1–3], which has led to glacier melting, sea level rise, climate change, ocean storms and other environment problems [4,5]. It affects the normal life order and poses a great threat to human beings. In addition, the Paris Agreement points out that the global net zero emission of greenhouse gasses should be achieved by the end of this century [6]. Therefore, it is an urgent need to prevent global warming by capturing CO_2 and reduce the man-made carbon cycle. Carbon capture, utilization and storage (CCUS) by chemical method is considered as one of the most effective ways to reduce greenhouse gasses in the short term [7,8]. Based on the concept of CCUS, the conversion of CO_2 into high value-added products by electrochemistry has aroused widespread interest in industry and academia [9].

Some non-electrochemical and relatively mature CO_2 capture methods have been applied in large-scale industrial applications [10], such as biological method [11,12], adsorption method [13,14], membrane method [15], ammonia absorption method [16,17] and low temperature capture [18]. However, these methods face challenges such as high energy consumption, limited environmental recycling sites, energy and materials loss of regenerated adsorbents [6,19,20].

CO_2 capture and transformation by electrochemical method could be used as an efficient solution to overcome these problems. Electrochemical method is not limited to capture the CO_2 from point sources, but also capture and transform the carbonate from air, ocean, waste gas and liquid. The modular nature of the electrochemical process could offer multiple cell stacks, resulting in low-

* Corresponding authors.
E-mail addresses: xujinyuntj@126.com (J. Xu), zhengchunming@tiangong.edu.cn (C. Zheng), sunxh@tju.edu.cn (X. Sun).
[1] These authors contributed equally to this work.

https://doi.org/10.1016/j.cclet.2022.108075
1001-8417/

cost structural materials for interconnections, gas diffusion layers and catalytic layers [21]. In addition, such BPMs for CO_2 capture could realize a smaller floor area and be easily scale-up as needed [22]. The catalytic efficiency of CO_2 capture and transformation dependents on the product distribution and the electrochemical capture ratio of CO_2 source [23], which shows the unique advantages of electrochemical method.

For the CO_2 capture and transformation of BPMs, the main driving force of the BPMs system is the electrochemical potential gradient. There is no need for external heat source or pressurization. Therefore, CO_2 capture could be carried out under isothermal condition by controlling the potential gradient [23,24], which is beneficial to reduce the demand for energy and cost. Usually, the acid-base capture of CO_2 by pH oscillation [25–27] and electrocatalytic reduction with transition metal (such as Zn [28], Cu [29,30] and Ni [31–33]) are two main approaches for electrochemical CCUS of CO_2 [23]. By the pH change of solution with the BPMs, CO_2 could be captured by local alkaline environment and finally converted into carbonate/bicarbonate, which CO_2 could be stored. As the reutilization of CO_2, the pH of the solution converted from high pH to low pH, the desorption of CO_2 could be realized under acid condition. Similar pH oscillation includes capacitive ion storage [34], proton coupled electron transfer (PCET) [35,36] and bipolar membrane electrodialysis (BPMED) [37,38].

Bipolar membrane (BPM) is a new kind of ion exchange membrane which could dissociate water into OH^- and H^+ by electrolysis [39]. BPM consists of anion exchange layer, cation exchange layer and catalytic layer (such as Al $(OH)_3$) between them [40,41]. When the BPMs is charged, the water molecules dissociated at the active sites of the catalytic layer into H^+ and OH^-. The high potential gradient would drive H^+ to the cathode through the cation exchange layer and OH^- to the anode through the anion exchange layer. Hence, bipolar membrane electrochemical device based on the concept of pH oscillation could be used for CO_2 capture (such as bipolar membrane electrodialysis (BPMED)) [42,43]. In recent years, the electrocatalytic reduction of CO_2 into different high value-added products using renewable energy sources as electricity has received increasing attention from researchers. The conventional H-type electrolytic cell for electrocatalytic CO_2 reduction has a current density of less than 100 mA/cm^2 due to the lower mass transfer limitation. The membrane electrode electrolyzer (MEA) combined with membrane technology is considered as a promising component for industrial CO_2 reduction due to its ability to provide higher current density and higher selectivity. However, at the same time, the type of membrane has a key influence on the current density and selectivity of MEA electrolyzer, such as cation exchange membranes (CEM) membrane electrode electrolyzer which provides high current density but also brings serious hydrogen precipitation reaction, and anion exchange membranes (AEM) membrane electrode electrolyzer which reduces hydrogen precipitation reaction while allowing the cathode product to cross over to the anode for re-oxidation. Since the BPMs could prevent the crossover of H^+ and OH^- and stabilize the pH value of electrolyte [44,45], thus improving ion transfer ability in electrolyte, electrochemical CO_2 reduction reaction (ECO_2RR) based on the BPMs could improve the electrochemical reduction performance of CO_2 [46]. However, commercial BPMs generally have non-negligible drawbacks such as high resistance, easy delamination and blistering. The thicker film layer is one of the reasons for the high resistance of BPMS compared to monopolar films [47]. Therefore, the fabrication of thinner anion exchange membrane (AEL) and cation exchange membrane (CEL) by improving BPMs thickness will result in high conductivity and selectivity of the overall BPMs, while decreasing delamination of BPMs requires improving AEL and CEL interfacial compatibility (*e.g.*, developing a three-dimensional CEL-AEL interface).

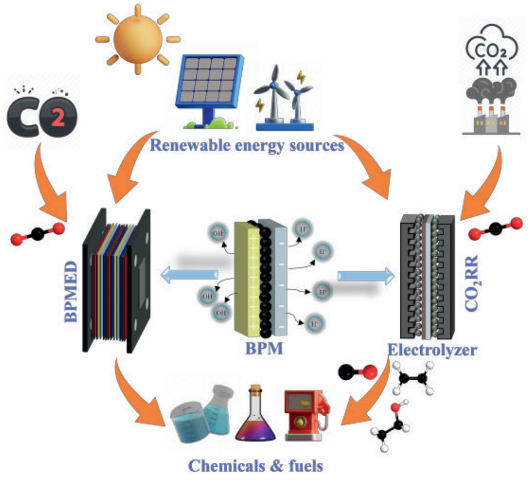

Fig. 1. Schematic diagram of electrochemical capture of CO_2 based on bipolar membrane.

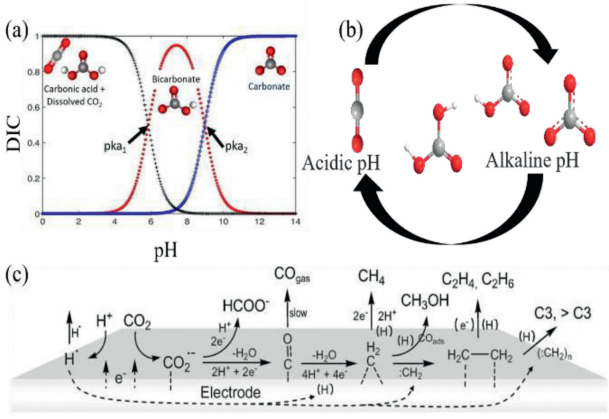

Fig. 2. (a) Relationship between carbon dioxide equilibrium and pH (for a closed system with a temperature of 25 °C and a salinity of 35 ppt). (b) Schematic diagram of pH fluctuations. Reproduced with permission [27]. Copyright 2020, Royal Society of Chemistry. (c) Reaction mechanism for the preparation of different products by electrochemical reduction of CO_2. Reproduced with permission [51]. Copyright 2007, Royal Society of Chemistry.

Thus, the active contact area and interfacial stability could be increased [48,49].

In general, the BPMs have great potential for electrochemical capture and utilization for CO_2 (Fig. 1). In this review, the bipolar membrane electrochemical capture and more robust CO_2 utilization processes are introduced in detail. Different types of BPM membranes and devices design are investigated and compared. In addition, the challenges and opportunities are also discussed for the development of the BPMs structure design and reductive equipment assembling for the CO_2 capture and transformation.

2. Basic reaction mechanism: pH oscillation and electrocatalytic reduction reaction

Bipolar membrane electrodialysis (BPMED) uses the pH swing of working fluid to capture and separate CO_2 at ambient temperature and pressure, and to recover CO_2 by continuously changing the pH value of working fluid between alkaline and acidic pH to affect CO_2 balance [27]. As shown in the Figs. 2a and b, be reversible and the recycling of CO_2 could be realized by changing the carbonate balance. Electrocatalytic reduction of CO_2 is much more complex reduction process than acid-base CO_2 capture with BPMs, which contains multiple charge transfer reactions, usually involving 2∼18 electron transfer pathways, many products, com-

Table 1
Reaction equations and electrode potentials of different reduction products [50].

Main reaction equation	Electrode potential (V *vs.* SHE)
$2H^+ + 2e^- \rightarrow H_2$	−0.42
$CO_2 + 2H^+ + 2e^- \rightarrow CO + H_2O$	−0.53
$CO_2 + 2H^+ + 2e^- \rightarrow HCOOH$	−0.61
$CO_2 + 4H^+ + 4e^- \rightarrow HCHO + H_2O$	−0.48
$CO_2 + 6H^+ + 6e^- \rightarrow CH_3OH + H_2O$	−0.38
$CO_2 + 8H^+ + 8e^- \rightarrow CH_4 + 2H_2O$	−0.24
$2CO_2 + 12H^+ + 12e^- \rightarrow C_2H_4 + 4H_2O$	−0.349
$2CO_2 + 12H^+ + 12e^- \rightarrow C_2H_5OH + 3H_2O$	−0.329

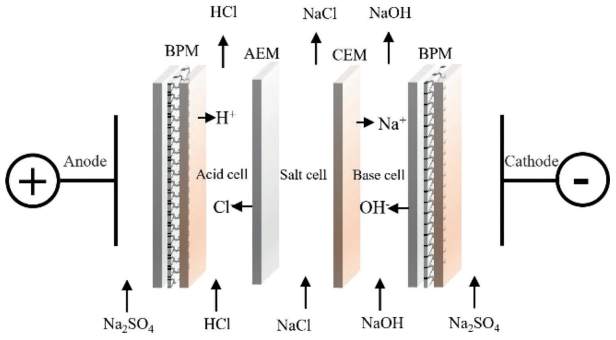

Fig. 3. Schematic diagram of B-C-A-B triple compartment bipolar membrane electrodialysis (BMED) unit for conversion of NaCl.

plex mechanism and high overpotential. The products include C_1 products (CO, CH_4, HCOOH, CH_3OH), C_2 products (C_2H_4, C_2H_5OH, C_2H_6, CH_3COOH, CH_3CHO) and C_3 products (C_2H_5CHO, C_3H_7OH), *etc.* Table 1 summarizes the main CO_2RR products at standard atmospheric pressure, 25 °C and the equilibrium potentials in aqueous solution with pH 7 (*vs.* SHE) [50]. CO_2 is first activated in aqueous solution into adsorbed CO_2(ads), and then CO_2(ads) is reduced by one electron to form CO_2 anion radicals ($\cdot CO_2^-$) (Fig. 2c). $\cdot CO_2^-$ is formed at potential of −1.90 V (*vs.* SHE), which is a key step to determine the reaction rate. After that, the C–O bond of the formed anion radical is broken and combined with protons or carbon atoms to form C–H or C–C bond [51]. When the Hg, Pb, In, Sn and other metals are used as catalyst, formic acid could be selectively generated, the oxygen of the anion radical coordinates with metal active center, and the carbon atom combines with proton to form C–H bond and get two electrons to form formate [52]. On the contrary, when Zn, Au, Ag and other metal catalysts are used, CO is selectively generated. The carbon atom of the anion radical coordinates with the active center of the metal catalysts [53]. When the Cu is used as catalyst, CO_2(ads) could be desorbed or further reduced by combining four electrons in the presence of protons, thus obtaining an adsorbed:CH_2 species. The surface methylene (:CH_2) reacts with two other electrons and protons to form CH_4, or with another :CH_2 to form ethylene [51].

3. Bipolar membrane electrodialysis (BPMED) method

When bipolar membranes are used with CEM and AEM, they could form BPMED with different compartments, which different compartments could convert salts in corresponding aqueous solutions to acids and bases (Fig. 3) [54]. BPMED could be used in the environmental protection to capture CO_2 from seawater [55], flue gas [56], atmosphere [6] and the solutions containing carbonates. With electrochemical pH oscillation, Bandi *et al.* use the BPMED to regenerate absorbent and capture CO_2 from air [42]. This method uses KOH solution to absorb CO_2 and the generated K_2CO_3 is acidified by sulfuric acid. Then, K_2CO_3 solution enters the BPMED unit, which alkaline washing solution and sulfuric acid were finally obtained. In addition, BPMED uses stacked structure, which makes it possible to obtain high purity for CO_2 capture. BPMED mainly uses two compartments and three compartments. Two compartments compose of B-C-B (BPM-CEM-BPM), B-A-B (BPM-AEM-BPM) and three compartments compose of B-C-A-B (BPM-CEM-AEM-BPM). Different membrane stack configurations of BPMED have great differences in energy consumption, efficiency, yield and product purity. The main characteristics of the two compartments are low energy consumption and small volume of compartments for acid and base. The main drawbacks of the three compartments are more membrane layer, high membrane resistance and high energy consumption. However, since the AEM and CEM do not directly contact with acid-alkali solution, the current efficiency and the product purity could be increased [57,58]. The specific methods would be discussed in detail for CO_2 capture in the next section.

3.1. Extract carbon dioxide from seawater

The ocean has absorbed about 40% of the anthropogenic carbon dioxide emitted since the industrial age [59,60], which its concentration is 2.1 mmol/kg [61], far exceeding the concentration (about 140 times) of carbon dioxide in the air [62]. This means that if CO_2 is captured from the air, a large volume of air would be processed, which brings significant cost challenges for carbon capture. However, the separation of carbon dioxide from the ocean by balancing total dissolved inorganic carbon (DIC) with the air would be an attractive way to capture carbon [63,64]. Carbon dioxide mainly exists in the form of HCO_3^- ions in the ocean. Electrodialysis (ED) has already proved that it could be used to recover carbon dioxide from electrodialysis of alkaline carbonate solution (Fig. 4a) [43,65]. However, this method with only ion exchange and no acidification to recover CO_2 has poor ion selectivity and low conductivity caused by diffusion and migration of carbonate/bicarbonate species, which are the main limitations of this method.

BPMED is expected to solve the shortage of electrodialysis. Bicarbonate/carbonate could be converted into H_2CO_3 (pH oscillation) by using the acid chamber in the bipolar membrane devices containing BPMs, and then extracted into CO_2 by membrane contactor in vacuum [25,27]. Based on this idea, Eisaman *et al.* [66] proposed a new prototype design, the constructed BPMED could efficiently extract dissolved inorganic carbon from seawater. The absorption rate of CO_2 could reach 59% with the electrochemical energy consumption of 242 kJ/mol (CO_2), as shown in Figs. 4b–d. However, hydrogen evolution (HER) and oxygen evolution (OER) occur simultaneously in the cathode and anode during the electrolysis process, which would lead to extra electrochemical energy loss. Digdaya *et al.* [26] further proposed to replace the original HER and OER in cathode and anode with reversible redox reaction.

Cyclically reversible redox coupling $K_3/K_4[Fe(CN)_6]$ solution was used as cathode and anode solution, thus significantly reduced polarization and electrochemical energy loss. The capture efficiency of CO_2 could reach 71% and the electrochemical energy consumption is 155.4 kJ/mol. However, the voltage drop with the BPMs is significant. The slow hydrodynamics causes the voltage loss.

In addition, another method of using BPMED to capture CO_2 in seawater is mineral carbonization, and CO_2 mineralization is beneficial in thermodynamics [55], which determines that it could capture CO_2 with lower cost and energy consumption. CO_2 mineralization is the chemical combination of CO_2 with Ca^{2+}/Mg^{2+} and other metal ions to form stable mineralized substances (such as $CaCO_3$, $MgCO_3$) [25,55]. In the process of capturing CO_2 and mineralizing metal ions, the system needs higher pH value (9.6–10) [67]. Compared with adding chemical alkali agents to the system, BPMED has shown the advantages of lower cost and no secondary pollution [55,68]. Zhao *et al.* [69] proposed a four-compartment bipolar membrane electrodialysis, as shown in Fig. 5a. Combined with calcium carbonate crystallizer, the problem of membrane fouling

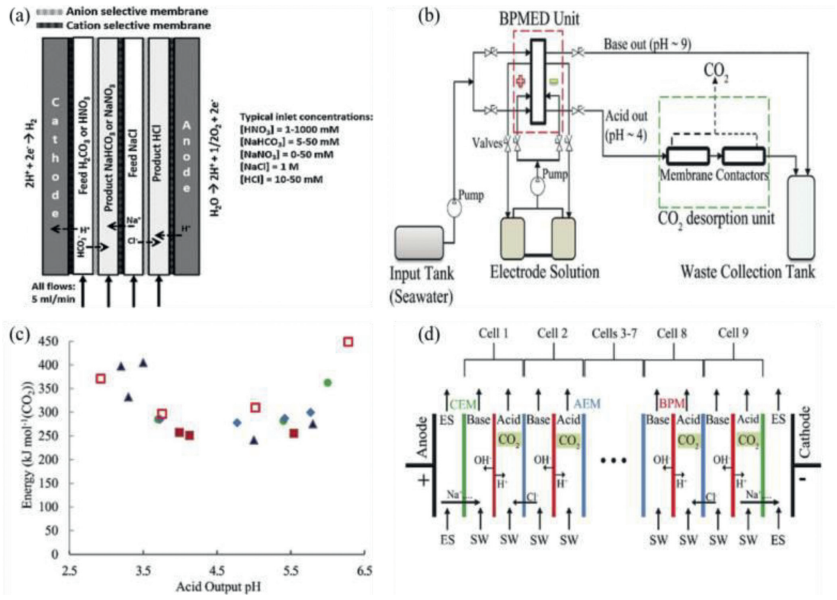

Fig. 4. (a) Removal of dissolved CO_2 and desalination of saline solution using electrodialysis cell. Reproduced with permission [65]. Copyright 2017, Elsevier. (b, c) BPMED schematics of CO_2 generation from seawater. (d) BPMED energy consumption for CO_2 generation from seawater. Reproduced with permission [66]. Copyright 2012, Royal Society of Chemistry.

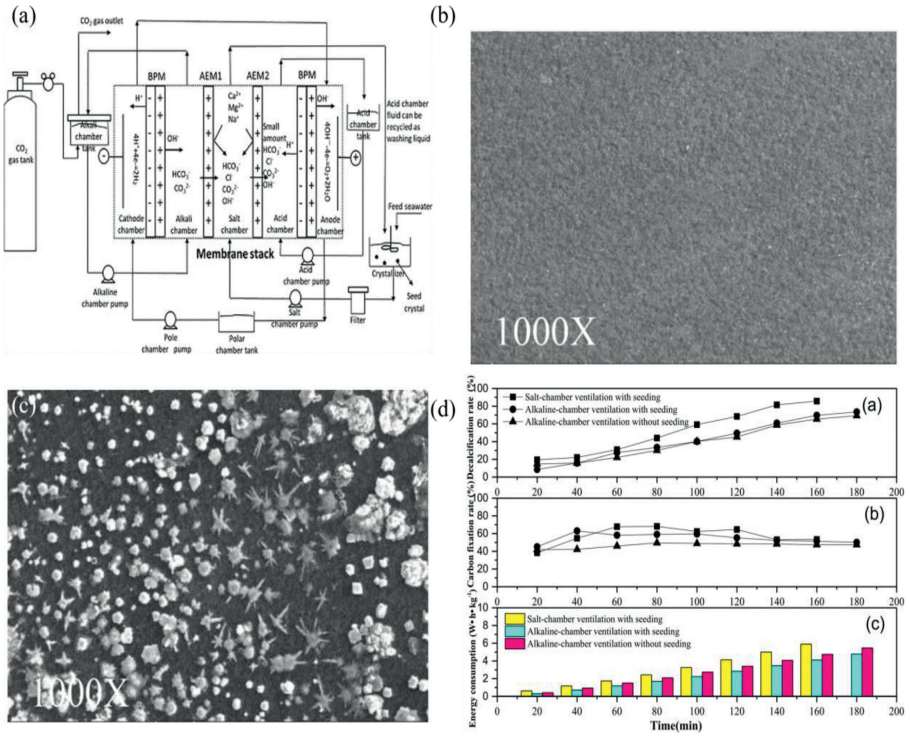

Fig. 5. (a) Schematic diagram of four-chamber bipolar membrane electrodialysis. AEM membrane surface SEM of salt chamber side under (b) alkali chamber ventilation and (c) salt chamber ventilation. (d) Trend charts of decalcification rate, carbon sequestration rate and energy consumption under different experimental conditions. Reproduced with permission [69]. Copyright 2020, Elsevier.

was solved, which decreased energy consumption during CO_2 carbonizing. Using cheap and easily available seawater, carbonate ions generated by CO_2 and BPMED alkali chamber migrate to salt chamber through cation exchange membrane, where they combine with seawater. The membrane pollutants are controlled to keep in ion state by adjusting CO_2 to enter alkali chamber instead of salt chamber. Meanwhile, hydroxide is consumed immediately and migrated to alkali chamber, which is one of the key factors to prevent membrane fouling. As shown in Figs. 5b and c, the $CaCO_3$ crystallizer and seed crystallization are also important to prevent membrane fouling. Experiments show that the fixation rate of CO_2 could reach 50.1%, and the decalcification rate could reach 73.4%. As shown in Fig. 5d, in addition, Zhao *et al.* [56] changed its gas-liquid contactor into a tower bubbling reactor by using the above system. The capture and utilization of acid gas (CO_2-SO_2) in flue gas were investigated. It was found that SO_2 in flue gas decreased carbon fixation rate, but increased decalcification rate. When current density was 12.5 A/m^2, gas velocity was 40 L/h and CO_2 in flue gas was 10%, carbon fixation rate was 31.4%, decalcification rate was 94.5%, and SO_2 in flue gas could be completely removed (100%).

Based on the above research results, to understand the operating mechanism of the process and to optimize the reaction conditions, Chen *et al.* [70] studied the competitive migration and reaction rate among OH^-, HCO_3^- and CO_3^{2-}, which experimentally determined the reaction rate of HCO_3^- and OH^- was greater than their migration rate. Therefore, the gas-liquid contact device could effectively improve the absorption rate of CO_2. By adding gas refining device, the aeration efficiency is greatly increased. Under the optimum conditions, the carbon fixation rate could reach 100% and the total energy consumption is 1.54 kWh/kg. Therefore, Sharifian *et al.* [71] directly pump seawater into the alkali chamber of BPEMD, instead of the previous capture mode with high purity alkali solution (high pH). 60% DIC and at least 16% Ca^{2+} were captured from seawater. The energy consumption for generating calcium carbonate was 0.88 kWh/kg. The irreversible overpotential of BPMs accounted for 55% of the theoretical value. However, membrane fouling is serious, which limits the large-scale use. To reduce the membrane fouling during the mineralization, development of bipolar membrane with optimized reaction kinetics and membrane thickness still remains a challenge.

3.2. Carbon sequestration by high pressure BPMED

When the bipolar membrane electrodialysis system captures CO_2 from seawater or carbonate solution, working under normal pressure and high current density would lead to CO_2 precipitation in the membrane stack, which would stay in the membrane stack and adhere to the membrane surface in the form of bubbles, thus affecting the actual effective membrane area of bipolar membrane electrodialysis. This would result in increased resistance, increased electrochemical energy consumption, damage to the membrane surface and decreased membrane life.

In addition, the concentration also determines whether CO_2 is precipitated or not [72]. Low concentration could effectively prevent gas from precipitating in the membrane stack and it also directly leads to the current density being reduced to 10 mA/cm^2 or even below. In order to solve this serious problem, Eisaman [72] and others proposed a high-pressure bipolar membrane electrodialysis. The designed device controls the pressure of acid, alkali and electrode solution by adjusting needle valves in the flow path, and adjusts the pressure in the range of 1.5–10 atm (Fig. 6). Experiments show that increasing the pressure could effectively prevent CO_2 precipitation in bipolar membrane electrodialysis stack. At a high current density of 139 mA/cm^2, the desorption energy at high voltage operation (6 atm) is reduced by 29% compared with that at approximately normal pressure operation (1.5 atm).

Furthermore, in order to accurately evaluate the high-pressure bipolar membrane electrodialysis proposed by Eisaman *et al.* and Sabatino *et al.* [6] used MATLAB to model the BPMED unit, in order to evaluate and improve the process performance by means of sensitivity analysis and process optimization. The data show that the model could well reproduce the experimental results, in which Eqs. 1 and 2 accurately describe the relationship between bubble generation and conductivity. The analysis shows that the rapid CO_2 generation rate would lead to the generation of CO_2 bubbles, the non-conductive phase would increase the resistance of the electrolytic cell, and the composition would also affect the conductivity, thus affecting the voltage drop of the electrolytic cell.

$$\frac{k^*_{\text{acid}}}{k_{\text{acid}}} = \frac{1 + AB\varphi_{CO_2}}{1 - B\gamma\varphi_{CO_2}} \quad (1)$$

$$\gamma = 1 + \frac{1 - \varphi_m}{\varphi_m^2}\varphi_{CO_2} \quad (2)$$

where A is the parameter of bubble shape, B is the parameter of its conductivity, φ_{CO2} is the volume fraction of CO_2 in the acid solution, and φ_m is the maximum volume fraction attainable [6].

3.3. Microbial fuel cell-bipolar membrane electrodialysis (BPMED-MFC)

Microbial electrochemical technology is a potential green method for sustainable production of electricity or chemical fuels [73]. Its sustainable energy recovery provides a broad prospect for electrochemical conversion of CO_2 into high value-added products [74]. CO_2 is a thermodynamically stable molecule with short bond length and high bond energy, so it needs high energy input to transform CO_2 molecules, which requires external energy to be carbon neutral, thus realizing green recovery of CO_2 [75]. Microbial fuel cell (MFC) is a typical microbial electrochemical system (MES), which could convert wastewater into renewable electricity by microorganisms. Combining MFC with electrodialysis of BPMs shows the potential of high cost-effectiveness and environmental friendliness for CO_2 capture [74,76].

Based on the concept of pH oscillation, CO_2 adsorption by alkali (NaOH) has the characteristics of low pressure and low energy consumption. Electrodialysis with BPMs could be integrated with MFC to produce alkali to capture CO_2 impurities in biogas, so as to purify biogas. Chen *et al.* [77] used MFC as power combined with BPMED to capture CO_2 in biogas in alkali production. As shown in Fig. 7, the bioconversion substrate on the anode of MFC is consumed by electricity-producing anaerobic microorganisms, which generate electrons and protons.

The electrons are transferred to the cathode electron acceptor through external resistance, and the protons are transferred to the cathode chamber through cation exchange membrane, thus providing power for BPMED. The research proves that the alkali solution prepared by BPMED-MFC has a good CO_2 capture effect, and the CH_4 concentration in biogas could reach 100%. However, the voltage required to use BPMs is higher than that generated by the device with biological cathode and anode. Therefore, it is necessary to provide additional energy from the outside [75], which has also been confirmed by Chen *et al.* [77]. Zhu *et al.* [75] designed a microbial reverse electrodialysis electrolysis and chemical production cell (MRECC), which uses reverse electrodialysis (RED) stack as power supply. This device could generate electricity through salinity gradient in wastewater [76,78], avoiding the usage for external voltage. This new MRECC system mineralizes CO_2 into carbonate products. Additional H_2 could be produced by combining the generated acids and bases with minerals, which would hopefully reduce the cost of capturing CO_2. The results show the cost of capturing CO_2 per ton is $25, which is lower than that of other mature methods.

Further, to recycle HCO_3^-/CO_3^{2-} ions formed by CO_2 absorption by alkali solution, Jin *et al.* [79] proposed a microbial electrolytic capture separation regeneration cell (MESC). The anode and cathode of the regeneration tank are separated by the BPMs and AEM, and the middle chamber is an acid chamber. BPMs keep the anode pH stable to prevent anode bacteria from growing. The generated H^+ migrates to the acid chamber through the cation exchange layer of BPMs, and the alkaline solution produced by the cathode is used to capture CO_2 in biogas. The generated HCO_3^-/CO_3^{2-} migrates to the acid chamber through AEM driven by potential difference to combine with H^+ for CO_2 regeneration. This combination of systems has been proven to be useful for capturing, separating and regenerating CO_2 from biogas, as well as for wastewater utilization. In addition, the newly proposed separation and regeneration system has a lower voltage for water decomposition than that of the abiotic electrolysis system. The results show the power consumption for biogas is 0.09 kWh/Nm^3. The H_2 generated at the cathode makes up about 27% of the cost.

Most of the reported BPMED-MFC systems use NaCl as electrolyte, which increases its operating costs. Therefore, seawater and high-salt wastewater could be combined in actual operating pro-

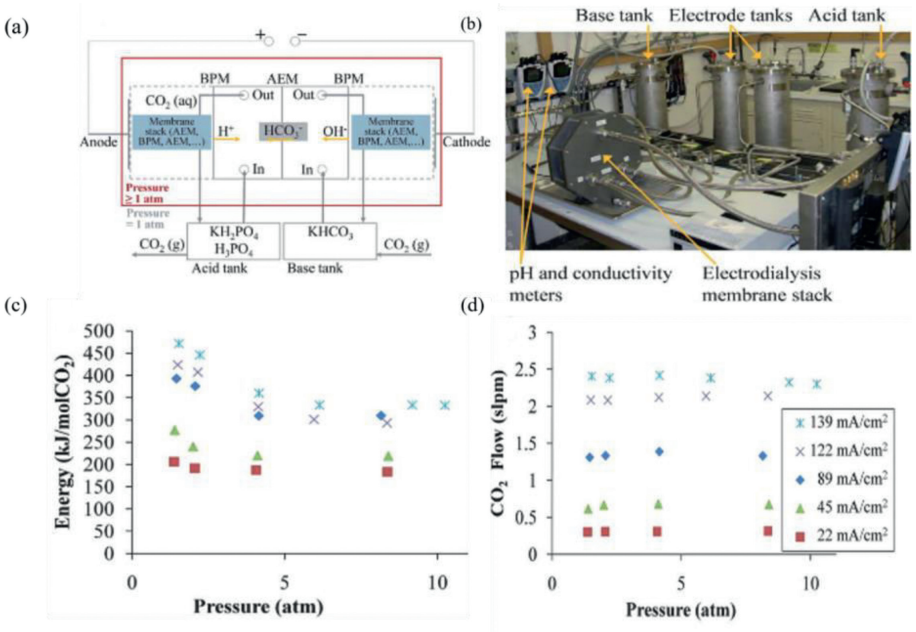

Fig. 6. (a, b) Schematic diagram of the high-pressure BPMED experimental setup used to solve CO. (c, d) Energy (kJ/mol CO_2) and CO_2 flow rate (slpm) *versus* pressure. Reproduced with permission [72]. Copyright 2011, Royal Society of Chemistry.

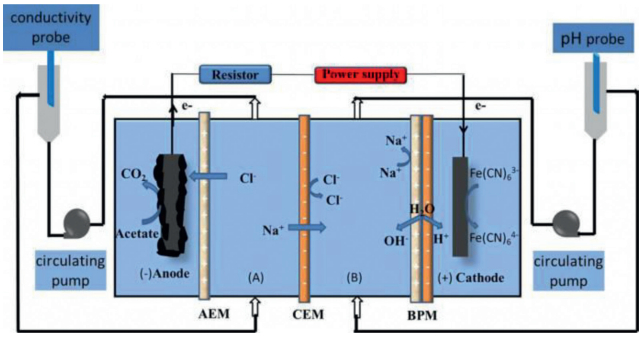

Fig. 7. Schematic diagram of the AEM-CEM-BPM configuration of the BPMED-MFC: (A) Desalination chamber and (B) alkali production chamber. Reproduced with permission [77]. Copyright 2013, Elsevier.

cess. In addition, wastewater could increase the conductivity of the working fluid, which could further reduce the operation cost. However, the selection and exploration of related materials have not been carried out, and its interference to other components in wastewater needs to be further explored, which still remains a challenge and an opportunity.

4. Electrocatalytic reduction method

Electrochemical CO_2 reduction reaction (CO_2RR) is another way to convert CO_2 into value-added fuels and high value-added chemicals by using renewable energy sources (wind energy and solar energy) [80,81], such as CO [82–84], formic acid [85], methanol [86], methane [87], ethylene [88,89], ethanol [90], acetic acid [91], propanol [92]. Energy storage in chemical products could reduce dependence on traditional fossil energy, thus reducing greenhouse gasses. It also helps to solve the problem of power misallocation due to seasonal and climatic factors [93]. In addition, CO_2RR system is modular structure. Its structure is relatively simple, which could be operated at normal temperature and pressure. Meanwhile, different reduction products can be changed by controlling the reduction potential.

The CO_2RR process is normally realized by an electrochemical CO_2 electrolytic cell, which is composed of a working electrode, a reference electrode and a three-electrode/two-electrode system. An ion exchange membrane is also used for separating the cathode chamber and the anode chamber to prevent the product from being reoxidized. In recent years, there are many studies on catalytic materials for electrochemical CO_2 reduction reaction electrode (CO_2RR). For C_1 products (such as formic acid, CO, methanol), Lin *et al.* [94] prepared homogeneous intermetallic Pd_3Bi nanocrystals by solvothermal method. Nearly 100% formate selectivity could be obtained for reversible hydrogen electrode at −0.35 V in 0.1 mol/L $KHCO_3$ solution. The crystal sequence of Pd and Bi atoms in the catalyst could inhibit the side reactions of CO. Ag is usually used for the electrochemical reduction of CO_2 to CO, however, monometallic catalysts suffer from slow kinetics, low product selectivity and poor stability, *etc.* Bimetallic catalysts made by doping with other metals are significantly different from monometallic catalysts. The newly doped metal of bimetallic catalysts not only changes the electronic structure of the raw material, but also provides more active sites and improves the structural stability of the active ingredient [95,96]. Zhang *et al.* [97] proposed a "two ships in a bottle" Zn-Ag-O ternary catalyst design (Figs. 8a–f), for the reduction of CO_2 to CO, achieving an energy efficiency of 60.9% and achieving a Faraday electrolysis efficiency of 94.1% ± 4.0% for CO (Figs. 8g–i). By thermodynamic DFT analysis and *in situ* X-ray absorption, it was shown that the delocalization of electrons stabilized the intermediate product *COOH, increasing the intrinsic CO activity and increasing the energy barrier for the formation of HCOO* and *H, thus inhibiting the occurrence of formic acid and hydrogen side reactions, resulting in enhanced selectivity for CO. Ren *et al.* [98] reported a strategy of implanting non-precious metal-active Sn-ZnO heterogeneous surfaces into the nanopores of high surface area carbon nanospheres (Sn-ZnO@HC, Figs. 9a–d) to reduce CO_2 to CO with a Faraday electrolysis efficiency of up to 91% at −0.53 V for CO and stability up to 240 h (Figs. 9e and f). With the help of density functional theory (DFT) and finite element method (FEM) calculations, the electronic interactions between Sn and ZnO reduced the Zn-d bandwidth and increased the Sn-d bandwidth, which facilitated the fracture of the *COOH inter-

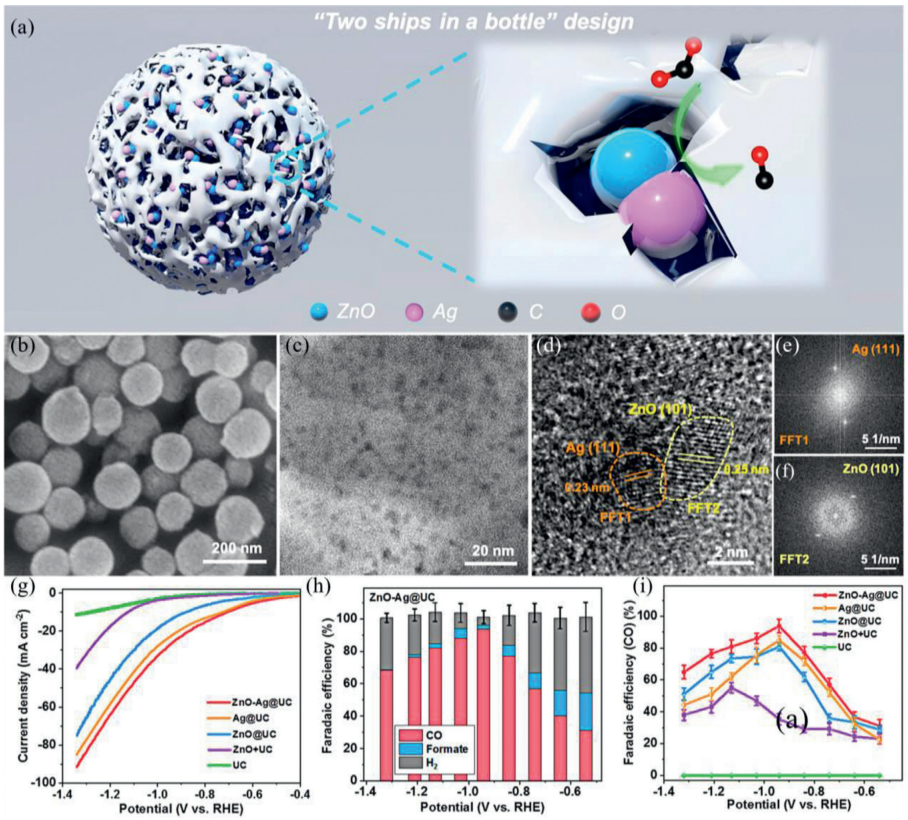

Fig. 8. "Two Ships in a Bottle" design concept and CO_2RR performance. (a) Schematic diagram of the "two ships in a bottle" catalyst. (b) SEM image of ZnO-Ag@UC. (c) TEM image of ZnO-Ag@UC. (d) HRTEM image of ZnO-Ag@UC. (e) Ag(111) and (f) ZnO(101). (g) LSV curve of catalyst. (h) FE distribution of ZnO-Ag@UC on product. (i) FE of catalyst on CO. Reproduced with permission [97]. Copyright 2021, American Chemical Society.

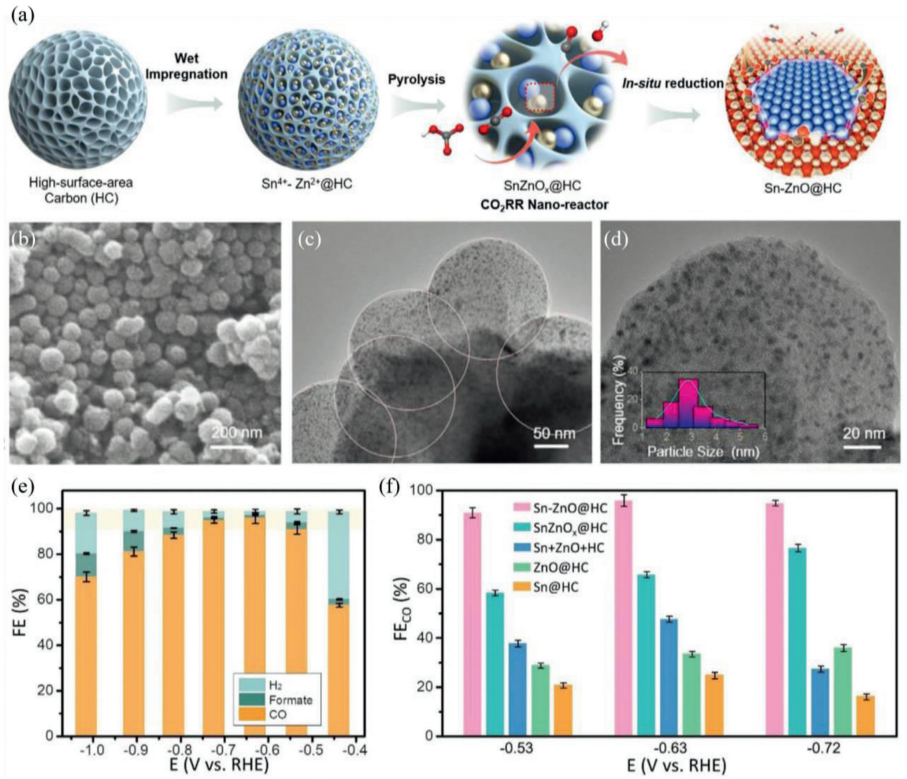

Fig. 9. (a) Schematic diagram of Sn-ZnO@HC catalyst preparation (blue, gold, red, white, and gray atoms represent Sn, Zn, O, H and C elements). (b) SEM image of Sn-ZnO@HC. (c) TEM image of Sn-ZnO@HC. (d) Histogram of size distribution. (e) FE distribution of Sn-ZnO@HC on reduction products. (f) FE of different catalysts on FE of the partial current density of CO. Reproduced with permission [98]. Copyright 2022, Wiley.

mediate. Hence, this bimetallic oxide heterostructure further promotes the CO_2 reduction reaction kinetics due to the mutual synergistic effect between the two metals [95]. Wei *et al.* [99] synthesized a multi-stage porous Ag nano-foam (AgNF) modified by SCN on Ag surface. The maximum faraday electrolysis efficiency of AgNF for CO reach 97%, which commonly maintains above 90% in the potential range of $-0.5 \sim -1.2$ V (*vs.* RHE). The main reason is the SCN ligand could promote the formation of COOH* intermediates by changing the local electron density on Ag surface. For C_2 products (such as ethylene, acetaldehyde), Zahid *et al.* [100] prepared oxidized derived copper (ODCu) electrode by hydrothermal method. The electrode has high selectivity for C_{2+} products, and the Faraday electrolysis efficiency of C_{2+} products could reach 58% at -0.95 V. Zhu *et al.* [101] prepared three-dimensional dendritic copper-cuprous oxide composites by reductive electrodeposition. The contact resistance between the electrocatalyst and composite matrix is almost zero. The dendritic structure helps to expose abundant active sites of Cu. Therefore, the overpotential for acetic acid and ethanol is only 0.53 V and 0.48 V. The Faraday electrolysis efficiency for C_2 products could reach over 80% at 11.5 mA/cm^2.

From above research, most research focused on cathodes and anodes preparation and performances for electrochemical reduction of CO_2. However, the assembling of electrocatalytic reduction of CO_2 system also need to be introduced, since the structure design of electrolytic cell is also a key factor which affects current density, product selectivity, Faraday electrolysis efficiency and so on [93,102]. The typical H-type electrolytic cell has simple structure and low cost, which could be widely used. The drawback of the H-type electrolytic cell is slow mass transfer, large electrode space and small electrode area. Hence, its current density is far from the current density required by industry ($\geq$ 200 mA/cm^2). Continuous flow electrolytic cell has the advantages of reducing the transfer path, and reducing the mass transfer limitation when used with gas diffusion layer (GDL) [45]. To increase the catalytic performance of continuous flow electrolytic cell, polymer electrolyte membrane plays an important role, which could be divided into cation exchange membranes/proton exchange membranes (CEMs) [103], AEMs [104,105] and BPMs [106], *etc.* These polymer electrolyte membranes could prevent cathodic reduction products (such as formic acid, ethanol) from diffusing and migrating to anode to be reoxidized, thus avoiding the problem of reducing electrolysis efficiency of electrolytic cell. Different membranes determine different transfer types, which would directly affect the selectivity of products and Faraday electrolysis efficiency. For example, anion exchange membrane AEM would transfer cathode reactants (CO_3^{2-}/HCO_3^-) to anode, thus reducing CO_2 conversion efficiency. Cation exchange membrane would make H^+ migrate to the cathode, resulting in cathode acidification environment, which is beneficial to the HER side reaction [103] and greatly reduces CO_2 conversion efficiency. Bipolar membrane is expected to solve these problems and provide a stable cathode/anode pH environment. Therefore, in this section, the influence of membrane properties on the selectivity and reduction efficiency of electrolytic cells is discussed. The structure and mass transfer of electrolytic cells with different cells design are compared and analyzed. The development of potential BPM-based electrolytic cells is emphatically summarized and discussed.

4.1. H-type electrolytic cell and microfluidic cell

Microfluidic electrolytic cell is composed of cathode gas diffusion electrode loaded with CO_2 reduction catalyst and anode gas diffusion electrode loaded with oxidation catalyst [107–109]. The two diffusion electrodes are separated by an extremely thin electrolyte channel. The distance is usually less than 1 mm. During electrochemical reduction, CO_2 gas enters the cathode and reaches

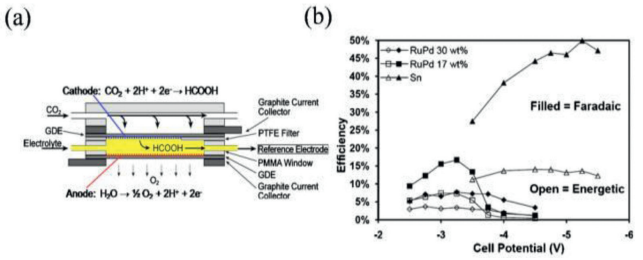

Fig. 10. (a) Schematic diagram of the microfluidic reactor used for CO_2 conversion. (b) Efficiency of different catalysts used in the microfluidic reactor. Filled symbols indicate Faraday efficiency, while open symbols indicate energy efficiency. Reproduced with permission [110]. Copyright 2010, Electrochemical Soc Inc.

the surface of gas diffusion electrode (GDE) to be reduced by cathode catalyst. O_2 produced by anode oxygen evolution is emitted into the air. Whipple *et al.* [110] first proposed a microfluidic reactor for electrochemical reduction of CO_2. As shown in Fig. 10a, an Ag/AgCl reference electrode is inserted into the electrolyte between two gas diffusion electrodes to detect the electrode potential. This reactor is used to quickly evaluate the catalyst and explore the influence of electrolyte pH on the reduction efficiency of carbon dioxide to formic acid. Experiments show that working at acidic pH value could significantly improve the performance of this electrolytic cell. When Sn/C is used as the cathode catalytic material, the Faraday efficiency (FE) of formic acid prepared by CO_2 is 89% and the energy efficiency reach 45% (current density 100 mA/cm^2). As shown in Fig. 10b, the flowing electrolyte flow is beneficial to change the pH and composition of electrolyte. The ultra-thin electrolyte channel also reduces the ohmic polarization loss of the cell. In addition, compared with the membrane-based flow cell, it could also reduce the permeation resistance of water molecules across the membrane and the concentration gradient caused by proton transfer across the membrane, thus avoiding the cathode flooding. Furthermore, Wu *et al.* [111] used microfluidic electrolyzer to reduce CO_2 to CO and established steady-state isothermal microfluidic cell mathematical model for microfluidic cell to reduce CO_2 to CO, which confirmed CO_2 reduction kinetics depends on CO_2 concentration at active sites to a great extent. This model is important to enhance CO_2 transfer rate to the catalytic layer (CL). In addition, CO_2 concentration in feed, gas feed flow rate, channel length and GDE porosity all have different effects on performance. Although microfluidic cell has great potential in electrochemical reduction of CO_2, it also has many drawbacks. Liquid reduction products produced in cathode would diffuse in electrolyte to anode and be reoxidized, which leads to the decrease of reduction efficiency.

In order to avoid the reduction products migrating to the anode and being reoxidized, the ion exchange separation membrane between the cathode and the anode is expected to solve this problem. Typical H-type electrolytic cell is still the most commonly used CO_2RR reactor in experiments. The cathode and anode chambers of H-type electrolytic cell are separated by an ion exchange membrane that only allows corresponding ions to pass through. The cathode chamber contains working electrodes and reference electrodes, and the anode chamber contains counter electrodes. The current density is usually less than 100 mA/cm^2 [112–114] due to the low solubility of CO_2 in water solution. In addition, the small electrode area and large electrode spacing also affect the overall electrolysis efficiency. Therefore, to overcome problems such as low mass transfer efficiency, it is necessary to adopt ultra-thin spacing and GDE of microfluidic cell. Ion exchange membrane also needs to be introduced to overcome the cross diffusion between cathode and anode products, which ensure continuous flow of electrolyte and reduce the limitation of CO_2 mass transfer, thus

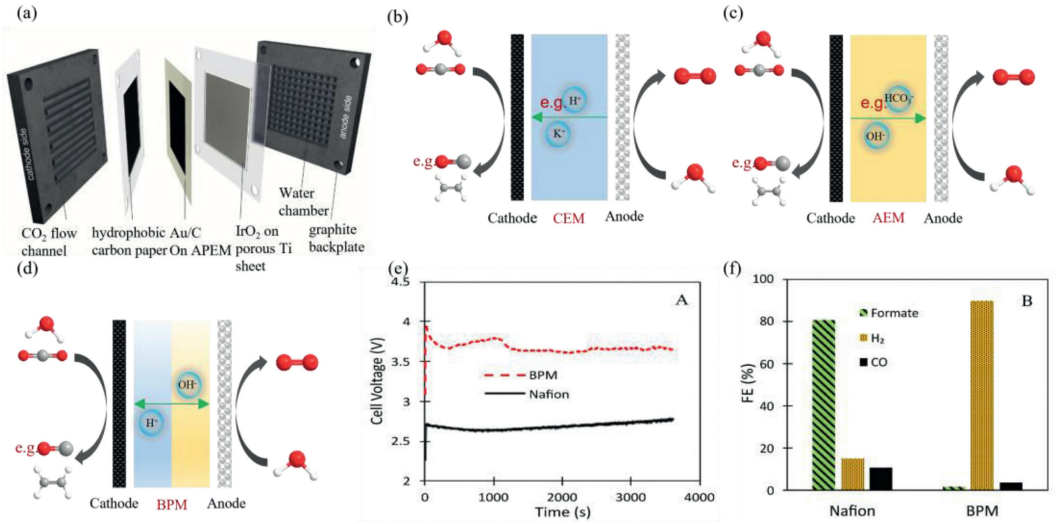

Fig. 11. (a–c) CEM, AEM and BPM ion transport mechanisms used for MEA configuration CO_2 reduction electrolytic cell. (d) Schematic diagram of the membrane electrode configuration electrolytic cell structure. Reproduced with permission [133]. Copyright 2019, Royal Society of Chemistry. (e) Comparison between the BPM-based and Nafion-based zero-gap electrolyzers in terms of timekeeping potential. (f) FE of analytical products of BPM-based and Nafion-based zero-gap electrolyzers. Reproduced with permission [124]. Copyright 2011, Wiley.

increasing the current density of the cells. The specific discussion would be presented in the next section.

4.2. CO_2 capture by MEA solid electrolyte

4.2.1. MEA configuration electrolytic cell based on CEM

Membrane electrode assembly (MEA) electrolytic cell is a new type of electrolytic cell. MEA electrolytic cell is a CO_2 reduction reactor formed by pressing polymer electrolyte membrane together with cathode and anode [115–117]. As shown in Fig. 11a, the continuously humidified CO_2 stream is directly supplied to the cathode. CO_2 reduction occurs at the boundary between the membrane and the cathode electrode. Gas-phase membrane-based CO_2RR reactor provides low current density by constructing electrochemical cells composed of membrane electrode assemblies (MEA), which solves the problem of low solubility and slow diffusion of CO_2 in water. Compared with liquid-phase CO_2RR reduction, it shows higher product selectivity and energy efficiency [45,115,118]. The addition of polymer electrolyte membrane effectively reduces the cross between reactants and products between cathode and anode, thus reduces the risk of catalyst poisoning caused by impurities in cathode electrolyte. Polymer electrolyte membranes used in MEA CO_2 reduction electrolytic cell are mainly divided into AEM, CEM and BPM, and their ion transfer mechanism is shown in Figs. 11b–d [119]. Delacourt *et al.* [103] first proposed the use of cation exchange membrane (Nafion®117) and the construction of MEA electrochemical cells. The cathode humidified CO_2 and the anode used pure water as electrolyte. At the current density of 20 mA/cm^2, no CO_2 reduction product was detected at the gas outlet, but the current efficiency of HER was close to 100%. The main reason is mainly due to the migration of H^+ from the anode to the cathode through the cation exchange membrane, which promoted the cathode selectivity to the side reaction of HER. In addition, it is also related to electrode poisoning and electrolyte property change. In order to alleviate the influence of acidic environment of cathode on CO_2RR, a 0.5 mol/L $KHCO_3$ buffer layer supported by glass fiber was introduced between cathode and cation exchange membrane [103]. At the same current density (20 mA/cm^2), the CO selectivity was greatly improved and the FE of CO was about 82%. The addition of buffer layer slowed down the arrival of H^+ to cathode, thus reducing the occurrence of HER. In addition, in the Nafion-based electrochemical cells, cations (such as K^+) would migrate from the anode side to the cathode in the Nafion-based electrolytic cell at pH < 1, which cations would affect the catalytic kinetics of CO_2RR [120,121]. In the process of CO_2RR based on proton exchange membrane using high concentration phosphate buffer (1 mol/L H_3PO_4), the increase of K^+ concentration would weaken the selectivity of HER. At the higher current density of 400 mA/cm^2, when local protons are exhausted (local pH > 7), the increase of K^+ concentration could tune the selectivity of HER to CO_2RR and increase the selectivity of CO_2RR [122]. The mechanism is that cations trigger CO_2 activation in the environment where protons almost disappear, thus inhibiting HER of water reduction [122,123]. On the other hand, the migration of metal cations from anode to cathode would cause the transfer of cathode electrolyte, which would increase the purification and separation cost of downstream electrolyte. In addition, metal cations migrating to the cathode would react with cathode carbonate and bicarbonate to form salt deposition at the interface between the membrane and the catalytic layer, thus preventing CO_2 gas from diffusing into the catalyst [124,125]. Adding sufficient water to the cathode could decrease salt deposition, but this would cause product dilution and GDE flooding in the cathode, which would limit the mass transfer of CO_2 and increase the cost of concentrating downstream products [126–128]. Therefore, improving water management system is a promising solution to salt deposition in CO_2RR based on cation exchange membrane. When the selective product is formic acid or formate, CEMs could prevent the migration of formate anions to the anode and prevent the product from being further oxidized at the anode [129,130]. In addition, the thickness of cation exchange membrane is low, so its potential drop in CO_2RR process is lower than that of other polymer electrolyte membranes (such as BPM) [131,132]. As shown in Figs. 11e and f, the initial cell potential of MEA configuration electrolytic cell based on bipolar membrane is 4 V, while the cell potential based on Nafion is 2.7 V [124]. Temperature also has an important influence on the voltage of CO_2RR electrolytic cell with MEA configuration. When the operating temperature of the electrolytic cell rises, the electrolytic cell voltage decreases [133].

When the cell temperature rises from 30 °C to 80 °C, the electrolytic cell voltage decreases from 2.5 V to 2.2 V, shown in Fig. 12a. The main reason is the kinetic effect of electrode reaction and ion conduction could be improved when the temperature increases. The reduction of high frequency resistance does not decrease the corresponding voltage potential (Fig. 12b). However, the

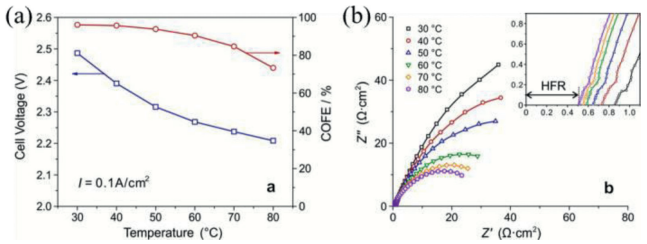

Fig. 12. (a) Effect of operating temperature on the reduction of MEA CO_2RR electrolytic cell to CO cell voltage and FE. (b) AC impedance spectrum recorded at open circuit voltage, inset zooms in on the high frequency region to show the variation of ion conduction with temperature. Reproduced with permission [133]. Copyright 2019, Royal Society of Chemistry.

increase of temperature would also adversely affect the membrane. Cation exchange membranes based on perfluorosulfonic acid (such as Nafion) have low proton conductivity at high temperature and could be decomposed [134,135]. In addition, fluorine-based membranes are complicated and expensive, hydrocarbon-based membranes could be an alternative design. The introduction of -SO_2H-group between carbon atom and sulfur atom of sulfonic acid group reduces the activation energy and increases the stability of the film. The main reason is that SO_2 is inserted between carbon atom and sulfur atom in neutral and anionic states, which leads to the withdrawal of electrons by SO_2 group and charge distribution, resulting in uniform and flat charge distribution [136]. Therefore, introducing highly electronegative groups between carbon atoms and sulfur atoms of sulfonic acid groups could be used as an important way to prepare fluorine-free hydrocarbon base membranes.

4.2.2. MEA configuration electrolytic cell based on AEM

MEA electrolytic cell based on AEM is more widely used than MEA electrolytic cell based on cation exchange membrane. On the one hand, AEMs prevent H^+ from migrating to the cathode catalyst surface through fixed cationic groups, thus avoiding undesired HER. On the other hand, AEMs transfer anions (such as OH^-) from cathode to anode through fixed cationic groups, and CO_2RR occurs in alkaline environment due to the continuous formation of cathode hydroxide. CO_2 stream would react with OH^- to form HCO_3^- and CO_3^{2-}. These anions would migrate to the anode through AEMs (called "cross"). Compared with OH^-, their charge mobility is lower and the transfer rate is slower, which leads to the decrease of ionic conductivity of AEMs [104]. HCO_3^- and CO_3^{2-} generated are neutralized by H^+ at the anode and converted back to CO_2 again. The neutralized CO_2 accounts for 50%–60% of the CO_2-consuming gas stream [105,137]. In addition, these anions crossed to the anode would be oxidized back to CO_2 at the anode [138,139] and mixed with the product O_2 of the anode, which makes this part of CO_2 unable to be directly reutilized and increases the cost of downstream gas separation. The standard potential at 298 K and relative to the standard hydrogen electrode (SHE) [E^0] [139] is summarized in Table 2. When the cathode target product is formate, the produced formate would also reach the anode electrolyte through AEMs, which reduces the concentration of the product and makes it difficult to purify the product [140].

Excessive water accumulation (water flooding) on porous electrodes is undesirable in the CO_2RR. Cathode flooding occurs when the amount of water transferred from anode to cathode exceeds the required amount of CO_2RR. The characteristics of AEMs are related to the water management of MEA electrolytic cell, and then affect the occurrence of flooding [119]. The use of low water absorption, thin AEM membrane ($\leq$ 40 μm) and hydrophobic cathode has been proved to reduce water flooding [141]. In addition, transmembrane transfer of water could promote the migration of cations (such as K^+) in cationic electrolyte across AEMs to cathode.

Table 2
Standard potentials for cathode and anode electrochemical reactions [139].

Cathode and anode electrochemical reactions	Standard electric potential (*vs.* SHE)
Cathode main reaction: $CO_2+2H^++2e^- \rightarrow CO+H_2O$ or $CO_2+H_2O+2e^- \rightarrow CO+2OH^-$	$E^0 = -0.103$ V
Cathode side reaction: $2H^++2e^- \rightarrow H_2$ or $2H_2O+2e^- \rightarrow H_2+2OH^-$	$E^0 = 0.000$ V
Anode main reaction: $H_2O \rightarrow H^++2e^-+\frac{1}{2}O_2$ or $2OH^- \rightarrow H_2O+2e^-+\frac{1}{2}O_2$	$E^0 = 1.229$ V
Anode side reactions: $2HCO_3^{2-} \rightarrow H_2O+\frac{1}{2}O_2+2e^-+2CO_2$ $CO_3^{2-} \rightarrow \frac{1}{2}O_2+2e^-+CO_2$	$E^0 = 0.765$ V $E^0 = 0.692$ V

These cations combine with cathode HCO_3^- and CO_3^{2-} and precipitate as K_2CO_3 and $KHCO_3$. The solubility of K_2CO_3 and $KHCO_3$ is lower than that of KOH, which would deposit on the surface of porous gas diffusion electrode. These precipitates hinder the reactants from reaching the catalyst layer and limit the migration of reactants, which affect the CO_2RR performance [104,142]. But cations at the cathode promote CO_2RR through local electrostatic effect [143,144]. Therefore, ideal AEMs hope to have high ionic conductivity, high ionic mobility and low permeability of products [93], thus reducing the occurrence of side reactions and improving the selectivity of products. Gabardo *et al.* [145] first proposed a strategy to apply AEMs to MEA (Figs. 13a and b), and to efficiently reduce CO_2 to C_{2+}while carbon nanoparticles and graphite powder sprayed on the cathode surface of the Cu nanoparticles were used to achieve efficient removal of the concentrated liquid products (ethanol and *n*-propanol) from the exit gas stream. The anode is made of titanium mesh loaded with IrO_2. This design strategy achieves 50% and 80% Faraday electrolysis efficiencies for C_2H_4 and C_{2+} products (Figs. 13c–e). For AEMs, developing AEMs with higher performance is in urgent need to improve CO_2 reduction efficiency. Zou *et al.* [146] successfully synthesized a series of BC-PDDA-OH^- (PDDA: diallyl dimethyl ammonium chloride) membranes with different mass ratios by impregnation, chemical crosslinking and ion exchange with bacterial cellulose (BC) membrane as skeleton and polyquaternary ammonium salt compound.

The results showed that when the mass ratio of BC to PDDA was 1:0.5, the ionic conductivity was 23.87 mS/cm. The ionic conductivity of OH^- was even higher (28.5 mS/cm) after soaking in 0.5 mol/cm $KHCO_3$ for 720 h. When these membranes are applied to the electrochemical reduction of CO_2, they have high selectivity for formate. As shown in Fig. 14, FE could reach 50.8%. The electrochemical performance is better than that of Nafion and basic A901 membranes in 0.5 mol/L $KHCO_3$/0.5 mol/L KOH electrolyte. The reason is that BC-PDDA-OH^- membrane could promote the kinetics of CO_2RR, inhibit HER and reduce the cross of formate products to anode, thus improving the performance of electrolytic cell. Wang *et al.* [147] reported a series of polymer composite AEMs based on polyvinyl alcohol and guar hydroxypropyl triammonium chloride (PGG). The effects of three functional groups in PGG membrane on the efficiency and selectivity of CO_2 reduction to formate were investigated. The performance of PGG-GT (GA and TCA as binary crosslinking agents) membrane containing thiophene group for formate was better than that of PGG-GT membrane containing dimethyl octanaldehyde and hydroxybenzyl group, and surpassed that of commercial Nafion 212 membrane. Similar to AEMs reported by Zou *et al.* [146], the high efficiency and selectivity of PGG-GT membranes for formate is mainly due to the higher ionic conductivity and lower product cross-over rate of PGG-GT containing thiophene groups, which could promote the ion transfer kinetics and inhibit HER during CO_2 reduction. Therefore, these different

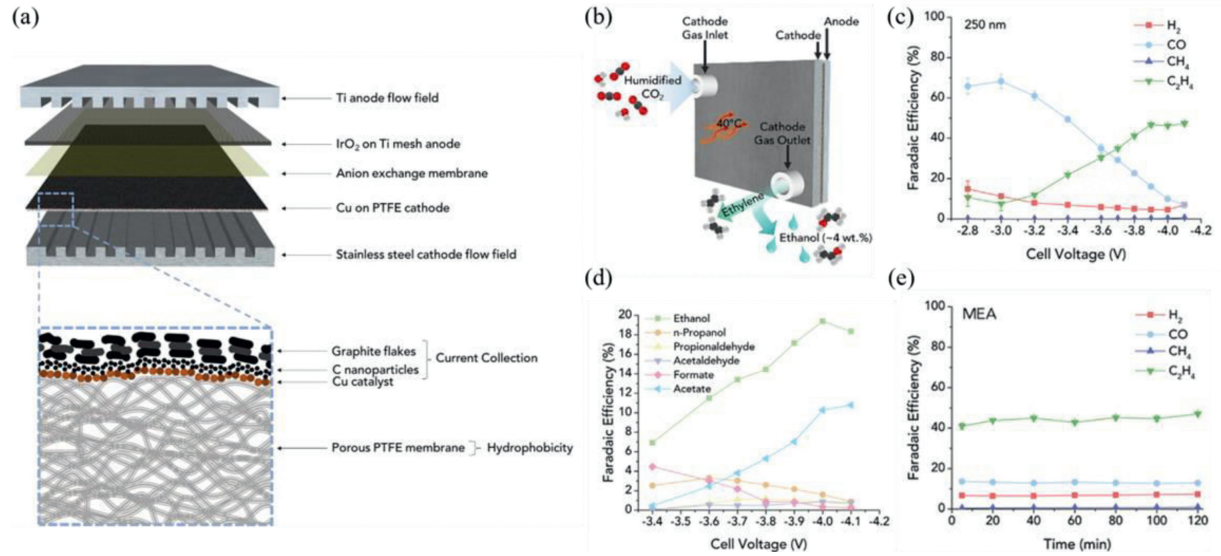

Fig. 13. Schematic diagram of the structure of AEM-MEA and its CO_2RR performance. (a) Schematic diagram of the local structure and cathode structure of AEM-MEA. (b) Schematic diagram of the overall AEM-MEA. (c) Product selectivity of 250 nm thick Cu catalyst layer. (d) Liquid product selectivity at different voltages. (e) Stability of the AEM-MEA electrolytic cell. Reproduced with permission [145]. Copyright 2019, Elsevier.

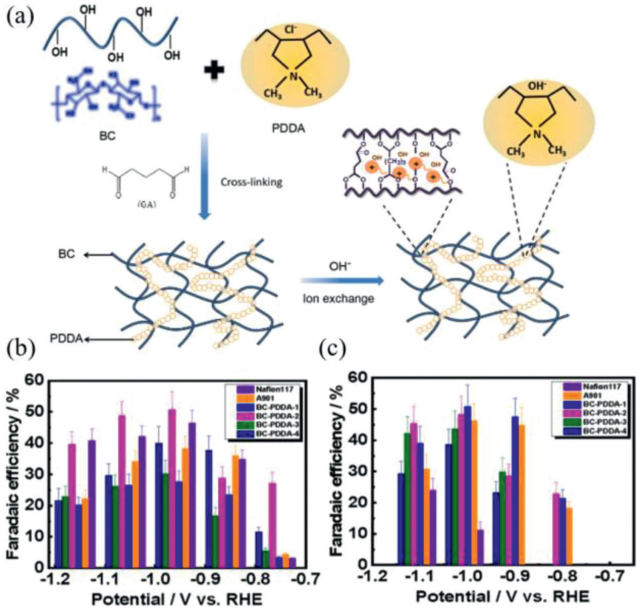

Fig. 14. (a) Material production process flow diagram and schematic diagram of the preparation process of BC-PDDA-OH^- membrane. (b, c) FE of different membranes under 0.5 mol/L $KHCO_3$ and 0.5 mol/L KOH electrolytes. Reproduced with permission [146]. Copyright 2021, Elsevier.

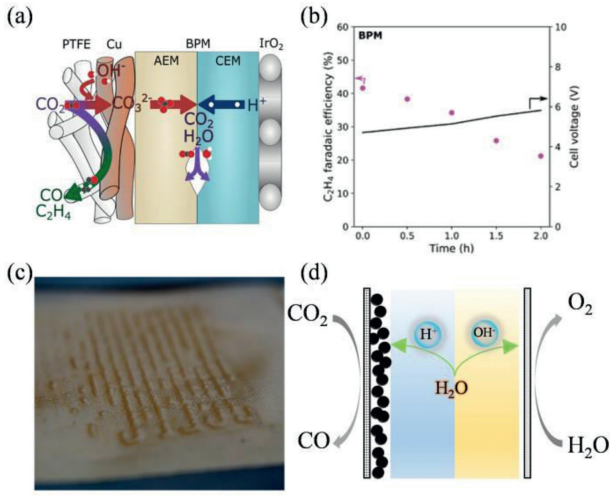

Fig. 15. (a) Schematic of species migration within the MEA with forward-biased BPM. (b) Voltage stability of C_2H_4 and forward-biased BPM at 50 mA/cm^2. (c) Photograph of BPM with forward-biased mode after running at 50 mA/cm^2 current density for 2 h. The BPM membrane blistered at the AEM: CEM interface. Reproduced with permission [88]. Copyright 2021, American Chemical Society. (d) Schematic diagram of species migration within the MEA with reverse-biased BPM. .

types of new AEMs have made new contributions to the scale-up of CO_2 electrochemical reduction.

4.2.3. MEA electrolytic cell based on BPM

Although AEM-based devices have a wide range of applications and excellent CO_2 electrochemical conversion performance, HCO_3^-/CO_3^{2-} species crossover from cathode to anode *via* AEM causes severe carbon loss. This has been identified as a major limitation of AEM-based devices [118,148]. MEA electrolytic cell with BPMs could prevent ion crossing better than that of AEMs electrolytic cell [75,106]. This BPMs-based electrolytic cell could work in two modes of "forward bias" and "reverse bias". When BPMs is in forward bias, CEL side of BPMs is close to anode with high potential and AEL side is close to cathode with low potential (Fig. 15a). AEL of BPMs could provide OH^- to the cathode. Meanwhile, it could provide an alkaline environment for the cathode and inhibit the HER without buffer layer [88]. Blommaert *et al.* [149] found that when BPMs was placed in forward bias mode, the Ag cathodic potential decreased 3 V at 25 mA/cm^2 compared with reverse bias mode since there was no water dissociation in the interlayer (Fig. 15b).

In addition, anions in the CEL are repelled by Donnan repulsion of fixed negative charge group in the layer (*e.g.*, sulfonic acid anion) driven by the potential difference [150]. The cations (*e.g.*, H^+) are transferred to the hydrolysis CL. Similarly, the anions (such as HCO_3^-/CO_3^{2-}) are transported to the CL layer through the AEL. These ions combine with cations (H^+) to form CO_2 and H_2O again, which leads to the stratification of AEL and CEL at the junction

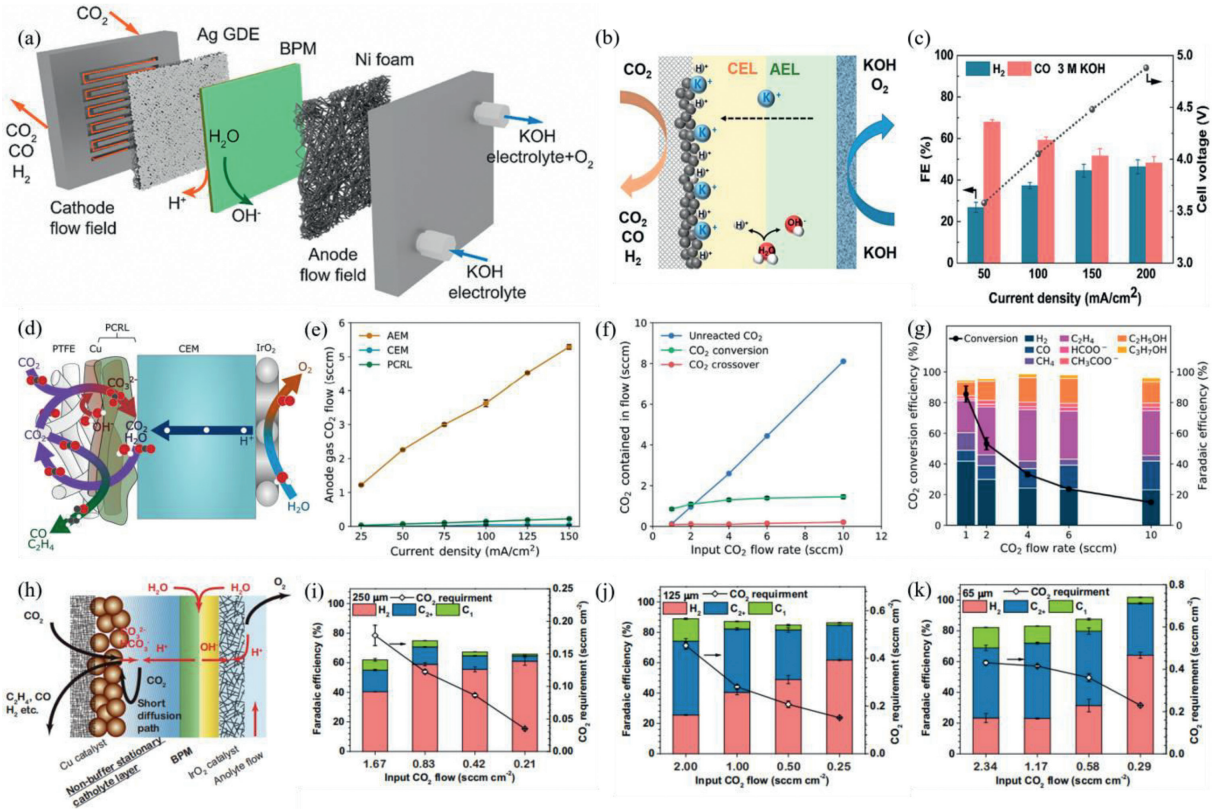

Fig. 16. Schematic diagram of different structures of BPM-MEA and their CO_2RR performance. (a) Schematic diagram of BPMEA structure with high concentration anode electrolyte. (b) Schematic diagram of ion transport in BPMEA system. (c) The relationship between different current densities and electrolytic cell voltages under 3 M KOH anode electrolyte and the FE for CO. Reproduced with permission [152]. Copyright 2021, American Chemical Society. (d) Schematic diagram of MEA with PCRL structure. (e) Comparison of CO_2 flux in PCRL anode with AEM and CEM. (f) CO_2 flux distribution at PCRL coating thickness of 2.25 mg/cm^2. (g) Conversion efficiency and FE distribution at 2.25 mg/cm^2 coating thickness. Reproduced with permission [88]. Copyright 2021, American Chemical Society. (h) Schematic diagram of SC-BPMEA structure and mass transfer. (i-k) FE distribution of products with different cathode liquid thickness. Reproduced with permission [153]. Copyright 2022, Springer Nature.

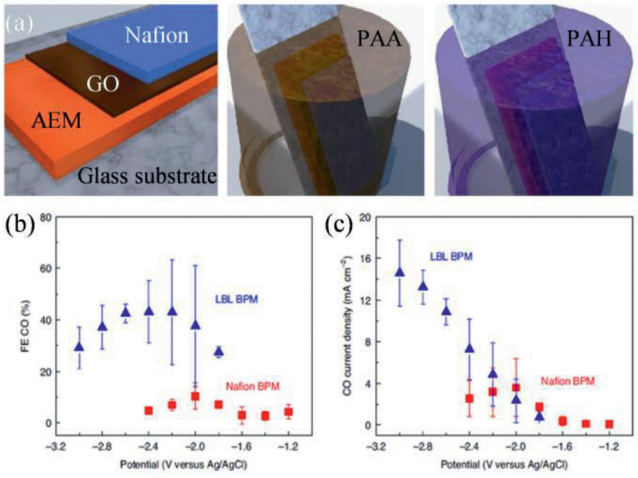

Fig. 17. (a) Schematic diagram of the modified BPM structure by LBL assembly. (b) CO FE *versus* cathodic potential for the ionomer-free catalyst layer. (c) CO fraction current density *versus* cathodic potential. Here the LBL BPM contains 10 PAH/PAA bilayers. the decrease in CO current density of Nafion BPM at higher potentials may be caused by water immersion in the ionomer-free catalyst layer. Reproduced with permission [81]. Copyright 2021, Springer Nature.

of the membrane, resulting in the decrease of stability (Fig. 15c). Hence, electrolysis efficiency and reactant CO_2 also decreased in the intermediate layer [88,118].

When BPMs is in reverse bias, the AEL side of BPMs is close to the anode with high potential, while the CEL side is close to the cathode with low potential. As shown in Fig. 15d, reverse bias is traditionally used to promote the dissociation of water and stabilize the pH values of electrochemical cells. In the reverse bias mode, hydrated ions migrate from the interface layer (IL) to both sides of the cathode and anode, thus depleting the moving charge on the film. To provide the required ion current and to keep the charge neutral, the dissociation of water could be further triggered [47]. The dissociation of water makes OH^- get alkaline environment through AEL, which avoids using noble metal OER catalysts (such as Pt and IrO_2) [46,92]. Abundant oxygen evolution catalysts on earth could be used, such as Ni and $FeNiO_x$. But at the same time, this also reduces the concentration of moving ions in the interface layer and increases the BPMs resistance [150,151].

Based on these characteristics of bipolar membranes, to break the limitation of 50% conversion of CO as a target product, Yang *et al.* [152] used Ag as cathode and nickel foam as anode with the help of BPMEA (Figs. 16a and b). A high concentration of KOH electrolyte was delivered at the anode to allow the anode cation (K^+) to cross the BPM to reach the cathode catalyst surface. The results showed that this approach improved the CO_2 reduction selectivity of the BPMEA system by a factor of 3, and the CO Faraday electrolysis efficiency reached 68% at a current density of 50 mA/cm^2 (Fig. 16c). Sinton *et al.* [88] developed permeable and renewable layer (PCRL) combined with CEMs for the instability of BPMs (Fig. 16d). This PCRL layer is made by spraying an anion-exchange ionomer solution (Aemion AP1-CNN5–00-X) to a certain loading level, which provided an alkaline environment on the catalyst surface combined with the acidic environment provided by CEMs. MEA CO_2 reduction electrolytic cell could be as-

Table 3
Comparison of different structure CO_2RR electrolytic cell development and design. CO_2 reduction reactor types.

CO_2 reduction reactor types	Carbonate balance	Current-density (mA/cm^2)	CO_2 conversion rate (%)	Advantages	Disadvantages	Refs.
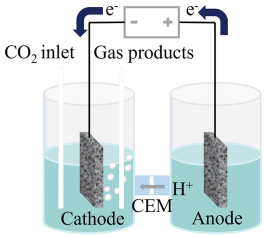	Loss in the cathode electrolyte	30	N/A	Simple device, easy to operate; cheap price; screening catalysts	Mass transfer limitation; low current density; difficult to apply on a large scale	[33]
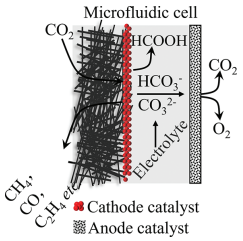	Loss in electrolyte microchannels; oxidized at the anode and combined with protons to revert to CO_2 again	100	45	Avoid flooding; avoid high membrane costs; higher mass transfer; small ohmic polarization loss	Product crossover; loss of output; increased cost of liquid product separation	[110]
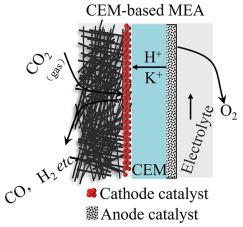	Revert to CO_2 on the CEM surface	100	N/A	Avoid re-oxidation of formate products; blocking anion migration; lower voltage drop compared to other electrolyte membranes	Promote HER, affect CO_2RR selectivity	[103]
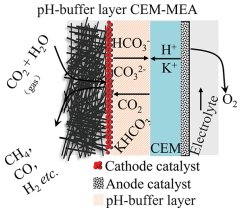	Revert to CO_2 near the CEM surface	100	N/A	Improved selectivity of the cathode for the reduction of CO_2 to CO; inhibition of HER	High resistance of electrolytic cell; electrolytes flushed out of the buffer layer; not applicable practical application	[103]
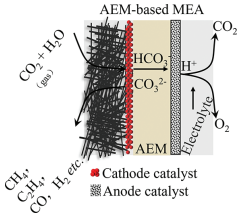	Carbonate migrated to the anode through AEM and was restored to CO_2 at the anode	100–200	30	Wide range of applications; block H^+ migration to the cathode; improved cathode product selectivity	Migration of carbonate ions to the anode; anode CO_2 loss	[145]
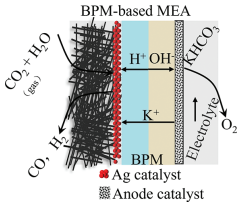	Revert to CO_2 on the CEL surface	200	50–60	Higher resistance to ion crossover; provide stable pH for cathode and anode; avoid the use of precious metal OER catalysts in the anode; highly reactive acid can be used to stabilize the cathode	Greater membrane resistance in reverse bias mode; The AEL and CEL of BPM are easily layered in forward bias mode	[152]

(*continued on next page*)

Table 3 (*continued*)

CO_2 reduction reactor types	Carbonate balance	Current-density (mA/cm^2)	CO_2 conversion rate (%)	Advantages	Disadvantages	Refs.
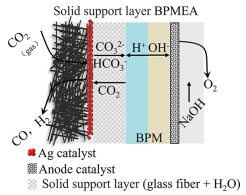	Revert to CO_2 on the CEL surface	200	N/A	Improved CO_2RR product selectivity; higher current density	Reduction of liquid phase product concentration	[45]
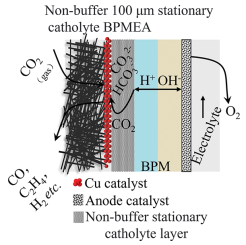	Recovery to CO_2 near about 12 μm at the cathode	300	78	Avoid loss of reactants from carbonate formation; elimination of energy loss associated with CO_2 loss in electrochemical CO_2 reduction; high CO_2 utilization	Porosity, structure and hydrophobicity of porous support layers need to be further optimized	[153]
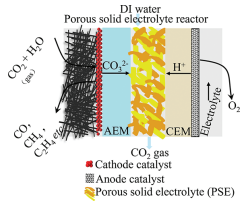	Revert to CO_2 on the porous solid electrolyte	200	> 90	Recovery of CO_2 gas for reuse without mixing with anode O_2; avoids the use of additional gas separation equipment; energy required to avoid the separation of cross-CO_2 from oxygen	Larger ohmic drop caused by larger solid electrolyte layer thickness; low ionic conductivity between cathode and anode	[105]

sembled with IrO_2 as anode and Cu catalyst as gas diffusion electrode. Local regeneration of CO_2 is realized, which is similar to the bipolar membrane structure, but avoids the undesired stratification of BPMs. The CO_2 crossover was controlled within 15% of the conversion product (Figs. 16e and f). The single CO_2 conversion rate reached 85% at 100 mA/cm^2 combined with low flow rate and low crossover, as shown in Fig. 16g. To address the previous limitation of only 25% single utilization of C_{2+} in neutral electrolytic cells, Xie *et al.* [153] designed an extremely thin cathode layer model (SC layer, consisting of a commercial porous support, material can be polyvinylidene difluoride (PVDF), poly tetra fluoroethylene (PTFE), polycarbonate (PC)) with the help of BPMEA, as shown in Fig. 16h. A porous support layer (2 cm × 2 cm, with different thicknesses) was placed on the cathode surfaces to achieve thin cathode, which was sonicated for 15 min in a saturated ideal electrolyte to degas before use. It is possible to limit the diffusion path length of CO_2 to 10 μm, and this cathode layer could recover CO_2 from the carbonate produced by the reaction, thus overcoming the problem of reactant loss in the carbonate. The combination of CuNPs cathode and IrO_2 anode achieves a single CO_2 utilization rate of 78%, while the highest current density is up to 300 mA/cm^2 (Figs. 16i–k). Wang *et al.* [105] reported a strategy of porous solid electrolyte reactor, a MEA CO_2 cell was constructed by forming a permeable ionic conductive sulfonated polymer electrolyte between AEM and PEM as a buffer layer with Ag nanowire as cathode and IrO_2 as anode. The cross carbonate could be combined with protons to form CO_2 gas again. Generated CO_2 could be recovered by flushing porous solid electrolytes (PSE) layer with deionized water. At the current of 200 mA/cm^2, the recovery of cross CO_2 and FECO could reach 90%. Mandal *et al.* [81] assembled strongly acidic CEL on polyelectrolyte layer by layer (LBL) containing polyacrylic acid/polyallylamine hydrochloride (PAH/PAA) and formed a weakly acidic layer with the function of cation exchanger, thus forming a new type of BPM. The combination of LBL BPMs and weak acid CEL in gas-supplied CO_2 electrolyte could inhibit HER activity and increase FE. As shown in Fig. 17, the FECO of LBL BPMs is higher than that of Nafion BPM. Its current density increases significantly at high potential.

To sum up, the design and synthesis of BPMs materials have an important impact on electrochemical reduction of CO_2. There is still plenty of room for designing more efficient BPMs. At the same time, to improve the performance of CO_2 reduction electrochemical cell, catalyst selectivity, electrolyte type and operating conditions should be considered as a whole.

5. Conclusions and prospects

Electrochemical CO_2 capture is more convenient, sustainable and efficient than non-electrochemical methods, which bipolar membranes could play an important role in affecting acid/base production, low ion crossover and resource recovery in the electrochemical CO_2 capture process. This paper provides a detailed review of the bipolar membrane electrochemical CO_2 capture and transformation processes design with comparative discussions of the types of membranes and device types. Table 3 summarizes the development and comparison of different CO_2RR reactor designs.

(1) Make CO_2 capture and electroreduction more efficient and selective. CO_2 process design are discussed in detail and the types of membranes and devices are also compared. BPMED changes the equilibrium absorption of CO_2 through pH oscillation. Combined with mineralized substances in seawater, it has broad application prospects for seawater desalination. However, membrane fouling could not be ignored. The generation of non-conductive phases such as CO_2 bubbles also leads to the increased overall resistance and external power consumption. Therefore, it is necessary to further optimize operating conditions and processes. Developing bipolar membranes with higher rate for water dissociation and optimal membranes thickness is also important to solve these problems.

As for the CO_2 reduction, the preparation of electrocatalysts is undoubtedly extremely important for the selectivity of electrocatalytic reduction of CO_2 and the Faraday electrolysis efficiency of the products. While designing the catalysts, the structure of different catalysts as well as the type of hybridization have important effects on the performance of catalysts for CO_2 reduction. For example, bimetallic catalysts have higher active sites and structural stability compared to monometallic catalysts, while the design of heterostructures also stimulates the mutual synergistic effect between metals to promote the kinetics of the reduction reaction. Another important aspect is the design of the electrochemical reduction electrolyzer. The BPMEA has advantages such as low ion crossover rate, stable cathode pH compared to other membrane electrode (AEM/CEM). In terms of product selectivity, suppression of unwanted HER generation could improve product selectivity. In addition, the BPM has a lower cathodic potential using forward bias than reverse bias. Reverse bias could have better water dissociation rate and CO_2RR stability compared to forward bias.

(2) Make CO_2 capture and electroreduction more facile and safer. The BPM-based reactor avoids the use of toxic or expensive chemicals for CO_2 capture by pH oscillation. Cheap, widely available, nontoxic solutions are used as feedstocks, such as sodium chloride and seawater. The modular stack reactor also increases the ease of CO_2 capture. The BPM-based CO_2RR reactor allows the use of inexpensive and widely available non-precious metal anodes, which avoids the use of expensive precious metal.

Overall, BPMs have great potential for bipolar membrane electrodialysis and CO_2RR electrolytic cells. The combination of bipolar membrane electrodialysis for on-site independent CO_2 capture and BPMs-based MEA electrocatalytic conversion of CO_2 to high value-added products is highly desired to achieve the goals of greenhouse gas reduction and sustainable energy, which may be a direction of exploration to combine the two into a continuous capture and conversion flow device. However, further studies are needed to understand their overall function. The structural modification of the bipolar membrane, such as coating the cationic membrane with polyelectrolyte or trying to expel CO_2 from the catalytic interlayer, could decrease cathode and anode layer decomposition and swelling during the electrolysis of bipolar membrane and increase the BPMs stability. In addition, the development of BPMs with high water dissociation rates, low ion crossover, strong interfacial stability and long lifetime is crucial for future electrochemical CO_2 capture and transformation.

Declaration of competing interest

The authors declare that they have no known competing financial interests or personal relationships that could have appeared to influence the work reported in this paper.

Acknowledgments

This research was funded by the National Natural Science Foundation of China (Nos. 52272303 and 52073212), the National Key Research and Development Program of China (No. 2018YFC1602400), the General Program of Municipal Natural Science Foundation of Tianjin (Nos. 17JCYBJC22700 and 17JCYBJC17000), and the State Scholarship Fund of China Scholarship Council (Nos. 201709345012 and 201706255009).

References

[1] W. Rong, H. Zou, W. Zang, et al., Angew. Chem. Int. Ed. 60 (2021) 466–472.
[2] N. Gaulin, P.Le Billon, Clim. Policy 20 (2020) 888–901.
[3] S. Nanda, S.N. Reddy, S.K. Mitra, et al., Energy Environ. Sci. 4 (2016) 99–122.
[4] J.H. Mercer, Nature 271 (1978) 321–325.
[5] S.H. Schneider, Science 244 (1989) 904-904.
[6] F. Sabatino, M. Mehta, A. Grimm, et al., Ind. Eng. Chem. Res. 59 (2020) 7007–7020.
[7] F. Rubiera, C. Pevida, Greenh. Gases 8 (2018) 396–397.
[8] F. Sha, N. Zhu, Y. Bai, et al., ACS Sustain. Chem. Eng. 4 (2016) 3032–3044.
[9] O.S. Bushuyev, P. De Luna, C.T. Dinh, et al., Joule 2 (2018) 825–832.
[10] A.S. Reis Machado, M. Nunes da Ponte, Curr. Opin. Green Sustain. Chem. 11 (2018) 86–90.
[11] A. Anand, S. Raghuvanshi, S. Gupta, Curr. Sustain. Renew. Energy Rep. 7 (2020) 40–47.
[12] I. Matito-Martos, C. Sepúlveda, C. Gómez, et al., Chem. Eng. J. 417 (2020) 128020.
[13] B. Feng, H. An, E. Tan, Energy Fuels 21 (2007) 426–434.
[14] R.S. Patil, D. Banerjee, C. Zhang, et al., Angew. Chem. Int. Ed. 55 (2016) 4523–4526.
[15] K. Xie, Q. Fu, G.G. Qiao, et al., J. Membr. Sci. 572 (2019) 38–60.
[16] L. Li, G. Puxty, M. Maeder, et al., Energy Fuels 33 (2019) 5377–5383.
[17] S. Ma, G. Chen, S. Zhu, et al., Appl. Energy 162 (2016) 354–362.
[18] S.S. Mostafa, J.D. Hedengren, K.M. Powell, Appl. Energy. 228 (2018) 577–592.
[19] M. Fasihi, O. Efimova, C. Breyer, J. Clean. Prod. 224 (2019) 957–980.
[20] D.W. Keith, G. Holmes, D. St. Angelo, et al., Joule 2 (2018) 1573–1594.
[21] H.K. Ju, G. Kaur, A.P. Kulkarni, et al., J. CO_2 Util. 32 (2019) 178–186.
[22] R.A. Shaw, T.A. Hatton, Int. J. Greenh. Gas Control. 95 (2020) 102878.
[23] S.E. Renfrew, D.E. Starr, P. Strasser, ACS Catal. 10 (2020) 13058–13074.
[24] B. Gurkan, X. Su, A. Klemm, et al., iScience 24 (2021) 103422.
[25] C.F. de Lannoy, M.D. Eisaman, A. Jose, et al., Int. J. Greenh. Gas Control. 70 (2018) 243–253.
[26] I.A. Digdaya, I. Sullivan, M. Lin, et al., Nat. Commun. 11 (2020) 4412.
[27] R. Sharifian, R.M. Wagterveld, I.A. Digdaya, et al., Energy Environ. Sci. 14 (2021) 781–814.
[28] J. Chen, Z. Li, X. Wang, et al., Angew. Chem. Int. Ed. 61 (2022) e202111683.
[29] T. Qin, Y. Qian, F. Zhang, et al., Chin. Chem. Lett. 30 (2019) 314–318.
[30] B. Wang, F. Yang, Y. Dong, et al., Chem. Eng. J. 396 (2020) 125255.
[31] Z.L. Wang, J. Choi, M. Xu, et al., ChemSusChem 13 (2020) 929–937.
[32] X. Yang, J. Cheng, B. Fang, et al., Nanoscale 12 (2020) 18437–18445.
[33] K. Xu, S. Zheng, Y. Li, et al., Chin. Chem. Lett. 33 (2022) 424–427.
[34] L. Legrand, Q. Shu, M. Tedesco, et al., J. Colloid Interface Sci. 564 (2020) 478–490.
[35] M. Rahimi, G. Catalini, M. Puccini, et al., RSC Adv. 10 (2020) 16832–16843.
[36] H. Xie, W. Jiang, T. Liu, et al., Cell Rep. Phys. Sci. 1 (2020) 100046.
[37] M.D. Eisaman, L. Alvarado, D. Larner, et al., Energy Environ. Sci. 4 (2011) 1045–1528.
[38] W. Ye, J. Huang, J. Lin, et al., Sep. Purif. Technol. 144 (2015) 206–214.
[39] Y. Wang, C. Huang, T. Xu, J. Membr. Sci. 374 (2011) 150–156.
[40] B. Bauer, F.J. Gerner, H. Strathmann, Desalination 68 (1988) 279–292.
[41] R. Pärnamäe, S. Mareev, V. Nikonenko, et al., J. Membr. Sci. 617 (2021) 118538.
[42] A. Bandi, M. Specht, T. Weimer, et al., Energy Convers. Manag. 36 (1995) 899–902.
[43] H. Nagasawa, A. Yamasaki, A. Iizuka, et al., AIChE J. 55 (2009) 3286–3293.
[44] Y.C. Li, D. Zhou, Z. Yan, et al., ACS Energy Lett. 1 (2016) 1149–1153.
[45] D.A. Salvatore, D.M. Weekes, J. He, et al., ACS Energy Lett. 3 (2017) 149–154.
[46] D.A. Vermaas, W.A. Smith, ACS Energy Lett. 1 (2016) 1143–1148.
[47] M.A. Blommaert, D. Aili, R.A. Tufa, et al., ACS Energy Lett. 6 (2021) 2539–2548.
[48] C. Shen, R. Wycisk, P.N. Pintauro, Energy Environ. Sci. 10 (2017) 1435–1442.
[49] Y. Chen, J.A. Wrubel, W.E. Klein, et al., ACS Appl. Polym. Mater. 2 (2020) 4559–4569.
[50] H. Cui, Y. Guo, L. Guo, et al., J. Mater. Chem. A 6 (2018) 18782–18793.
[51] G. Centi, S. Perathoner, G. Win, et al., Green Chem. 9 (2007) 671.
[52] J.S. Yoo, R. Christensen, T. Vegge, et al., ChemSusChem 9 (2016) 358–363.
[53] L.I. Bingyu, Q. Mao, J. Zhao, et al., Chem. Eng. Prog. 38 (2019) 4901–4910.
[54] A.J.B. Kemperman, Handbook On Bipolar Membrane Technology (Chinese version), Chemical Industry Press, Beijing, 2004.
[55] H. Xie, B. Liang, H. Yue, et al., Chem 4 (2018) 24–26.
[56] Y. Zhao, L. Wang, Z. Ji, et al., Desalination 494 (2020) 114654.
[57] Y. Li, S. Shi, H. Cao, et al., Water Res. 89 (2016) 201–209.
[58] Y. Wang, N. Zhang, C. Huang, et al., J. Membr. Sci. 385-386 (2011) 226–233.

[59] T. DeVries, M. Holzer, F. Primeau, Nature 542 (2017) 215–218.
[60] C.L. Sabine, T. Tanhua, Ann. Rev. Mar. Sci. 2 (2010) 175–198.
[61] N.R. Bates, Front. Mar. Sci. 5 (2018) 398.
[62] J.N. Butler, Carbon Dioxide Equilibria Their Applications, Routledge, United States, 1982.
[63] H.D. Willauer, F. DiMascio, D.R. Hardy, et al., Ind. Eng. Chem. Res. 51 (2012) 11254–11260.
[64] H.D. Willauer, F. DiMascio, D.R. Hardy, et al., Ind. Eng. Chem. Res. 53 (2014) 12192–12200.
[65] S. Dara, M. Lindstrom, J. English, et al., J. CO_2 Util. 19 (2017) 177–184.
[66] M.D. Eisaman, K. Parajuly, A. Tuganov, et al., Energy Environ. Sci. 5 (2012) 7346.
[67] W. Wang, M. Hu, Y. Zheng, et al., Ind. Eng. Chem. Res. 50 (2011) 8333–8339.
[68] E. Koivisto, R. Zevenhoven, Entropy 21 (2019) 395.
[69] Y. Zhao, J. Wang, Z. Ji, et al., Chem. Eng. J. 381 (2020) 122542.
[70] T. Chen, Y. Zhao, Y. Zhao, et al., ACS Sustain. Chem. Eng. 9 (2021) 8372–8382.
[71] R. Sharifian, L. Boer, R.M. Wagterveld, et al., Chem. Eng. J. 438 (2022) 135326.
[72] M.D. Eisaman, L. Alvarado, D. Larner, et al., Energy Environ. Sci. 4 (2011) 4031–4037.
[73] Y. Zhang, I. Angelidaki, Water Res. 56 (2014) 11–25.
[74] Y. Tian, D. Li, C. Li, et al., Chem. Eng. J. 414 (2021) 128671.
[75] X. Zhu, M.C. Hatzell, B.E. Logan, Environ Sci. Technol. Lett. 1 (2014) 231–235.
[76] X. Li, I. Angelidaki, Y. Zhang, Water Res. 142 (2018) 396–404.
[77] M. Chen, F. Zhang, Y. Zhang, et al., Appl. Energy 103 (2013) 428–434.
[78] X. Zhu, M.C. Hatzell, R.D. Cusick, et al., Electrochem. Commun. 31 (2013) 52–55.
[79] X. Jin, Y. Zhang, X. Li, et al., Environ. Sci. Technol. 51 (2017) 9371–9378.
[80] H. Shen, Y. Wang, T. Chakraborty, et al., ACS Catal. 12 (2022) 5275–5283.
[81] Z. Yan, J.L. Hitt, Z. Zeng, et al., Nat. Chem. 13 (2021) 33–40.
[82] C.M. Gabardo, A. Seifitokaldani, J.P. Edwards, et al., Energy Environ. Sci. 11 (2018) 2531–2539.
[83] S. Verma, Y. Hamasaki, C. Kim, et al., ACS Energy Lett. 3 (2017) 193–198.
[84] S. Verma, X. Lu, S. Ma, et al., Phys. Chem. Chem. Phys. 18 (2016) 7075–7084.
[85] B. De Mot, J. Hereijgers, N. Daems, et al., Chem. Eng. J. 428 (2022) 131170.
[86] N. Kumar, N. Seriani, R. Gebauer, Phys. Chem. Chem. Phys. 22 (2020) 10819–10827.
[87] A.I. Tsiotsias, N.D. Charisiou, I.V. Yentekakis, et al., Nanomaterials 11 (2020) 28.
[88] C.P. O'Brien, R.K. Miao, S. Liu, et al., ACS Energy Lett. 6 (2021) 2952–2959.
[89] D. Ren, Y. Deng, A.D. Handoko, et al., ACS Catal. 5 (2015) 2814–2821.
[90] J. Yuan, J.J. Zhang, M.P. Yang, et al., Catalysts 8 (2018) 171.
[91] C. Genovese, C. Ampelli, S. Perathoner, et al., Green Chem. 19 (2017) 2406–2415.
[92] M. Ma, K. Djanashvili, W.A. Smith, Angew. Chem. Int. Ed. 55 (2016) 6680–6684.
[93] D. Ma, T. Jin, K. Xie, et al., J. Mater. Chem. A 9 (2021) 20897–20918.
[94] L. Jia, M. Sun, J. Xu, et al., Angew. Chem. Int. Ed. 60 (2021) 21741–21745.
[95] Q. Li, Y.C. Wang, J. Zeng, et al., Rare Met. 40 (2021) 3442–3453.
[96] Y. Jia, F. Li, K. Fan, et al., Adv. Powder Mater. 1 (2022) 100012.
[97] Z. Zhang, G. Wen, D. Luo, et al., J. Am. Chem. Soc. 143 (2021) 6855–6864.
[98] B. Ren, Z. Zhang, G. Wen, et al., Adv. Mater. 34 (2022) e2204637.
[99] L. Wei, H. Li, J. Chen, et al., ACS Catal. 10 (2019) 1444–1453.
[100] A. Zahid, A. Shah, I. Shah, Nanomaterials 12 (2022) 1380.
[101] Q. Zhu, X. Sun, D. Yang, et al., Nat. Commun. 10 (2019) 3851.
[102] J.J. Wang, X.P. Li, B.F. Cui, et al., Rare Met. 40 (2021) 3019–3037.
[103] C. Delacourt, P.L. Ridgway, J.B. Kerr, et al., J. Electrochem. Soc. 155 (2008) B42–B49.
[104] N. Ziv, W.E. Mustain, D.R. Dekel, ChemSusChem 11 (2018) 1136–1150.
[105] J.Y.T. Kim, P. Zhu, F.Y. Chen, et al., Nat. Catal. 5 (2022) 288–299.
[106] Y.C. Li, Z. Yan, J. Hitt, et al., Adv. Sustain. Syst. 2 (2018) 1700187.
[107] B.A. Rosen, A. Salehi-Khojin, M.R. Thorson, et al., Science 334 (2011) 643–644.
[108] M.R. Thorson, K.I. Siil, P.J.A. Kenis, J. Electrochem. Soc. 160 (2012) F69–F74.
[109] C.E. Tornow, M.R. Thorson, S. Ma, et al., J. Am. Chem. Soc. 134 (2012) 19520–19523.
[110] D.T. Whipple, E.C. Finke, P.J.A. Kenis, Electrochem. Solid-State Lett. 13 (2010) B109–B111.
[111] K. Wu, E. Birgersson, B. Kim, et al., J. Electrochem. Soc. 162 (2015) F23–F32.
[112] S. Garg, M. Li, A.Z. Weber, et al., J. Mater. Chem. A 8 (2020) 1511–1544.
[113] J. Liu, P. Li, J. Bi, et al., Chemistry (Easton) 28 (2022) e202200242.
[114] D.M. Weekes, D.A. Salvatore, A. Reyes, et al., Acc. Chem. Res. 51 (2018) 910–918.
[115] F.P. Garcia de Arquer, C.T. Dinh, A. Ozden, et al., Science 367 (2020) 661–666.
[116] X. Wang, Z. Wang, F.P. García de Arquer, et al., Nat. Energy 5 (2020) 478–486.
[117] L.C. Weng, A.T. Bell, A.Z. Weber, Energy Environ. Sci. 12 (2019) 1950–1968.
[118] A. Pătru, T. Binninger, B. Pribyl, et al., J. Electrochem. Soc. 166 (2019) F34–F43.
[119] E.W. Lees, B.A.W. Mowbray, F.G.L. Parlane, et al., Nat. Rev. Mater. 7 (2021) 55–64.
[120] A. Murata, Y. Hori, Bull. Chem. Soc. Jpn. 64 (1991) 123–127.
[121] S. Ringe, E.L. Clark, J. Resasco, et al., Energy Environ. Sci. 12 (2019) 3001–3014.
[122] J.E. Huang, F. Li, A. Ozden, et al., Science 372 (2021) 1074–1078.
[123] C.J. Bondue, M. Graf, A. Goyal, et al., J. Am. Chem. Soc. 143 (2021) 279–285.
[124] B. De Mot, M. Ramdin, J. Hereijgers, et al., ChemElectroChem 7 (2020) 3839–3843.
[125] M.A. Izquierdo-Gil, V.M. Barragán, J.P.G. Villaluenga, et al., Chem. Eng. Sci. 72 (2012) 1–9.
[126] P. Jeanty, C. Scherer, E. Magori, et al., J. CO_2 Util. 24 (2018) 454–462.
[127] P. Tiwari, G. Tsekouras, G.F. Swiegers, et al., ACS Appl. Mater. Interfaces 10 (2018) 28176–28186.
[128] G. Díaz-Sainz, M. Alvarez-Guerra, J. Solla-Gullón, et al., J. CO_2 Util. 34 (2019) 12–19.
[129] L. Li, A. Ozden, S. Guo, et al., Nat. Commun. 12 (2021) 5223.
[130] W. Ma, S. Xie, X.G. Zhang, et al., Nat. Commun. 10 (2019) 892.
[131] T. Luo, S. Abdu, M. Wessling, J. Membr. Sci. 555 (2018) 429–454.
[132] H. Strathmann, A. Grabowski, G. Eigenberger, Ind. Eng. Chem. Res. 52 (2013) 10364–10379.
[133] Z. Yin, H. Peng, X. Wei, et al., Energy Environ. Sci. 12 (2019) 2455–2462.
[134] M. Rikukawa, K. Sanui, Prog. Polym. Sci. 25 (2000) 1463–1502.
[135] A.L. Rusanov, D. Likhatchev, P.V. Kostoglodov, et al., Proton-exchanging electrolyte membranes based on aromatic condensation polymers, in: G. Sunny (Ed.), Inorganic Polymeric Nanocomposites and Membranes, Springer Berlin Heidelberg, Berlin, 2005, pp. 83–134.
[136] F. Akinori, S. Hironori, T. Takashi, Comput. Theor. Chem. 1121 (2017) 44–48.
[137] G.O. Larrazabal, P. Strom-Hansen, J.P. Heli, et al., ACS Appl. Mater. Interface 11 (2019) 41281–41288.
[138] S. Fierro, L. Ouattara, E.H. Calderon, et al., Electrochim. Acta 54 (2009) 2053–2061.
[139] J. Herranz, A. Pătru, E. Fabbri, et al., Curr. Opin. Electrochem. 23 (2020) 89–95.
[140] M. Ma, E.L. Clark, K.T. Therkildsen, et al., Energy Environ. Sci. 13 (2020) 977–985.
[141] A. Reyes, R.P. Jansonius, B.A.W. Mowbray, et al., ACS Energy Lett. 5 (2020) 1612–1618.
[142] D.G. Wheeler, B.A.W. Mowbray, A. Reyes, et al., Energy Environ. Sci. 13 (2020) 5126–5134.
[143] S. Ringe, E.L. Clark, J. Resasco, et al., Energy Environ. Sci. 12 (2019) 3609–3610.
[144] B. Endrodi, A. Samu, E. Kecsenovity, et al., Nat. Energy 6 (2021) 439–448.
[145] C.M. Gabardo, C.P. O'Brien, J.P. Edwards, et al., Joule 3 (2019) 2777–2791.
[146] Q. Zou, X. Guo, L. Gao, et al., Sep. Purif. Technol. 272 (2021) 118910.
[147] M. Wang, N. Preston, N. Xu, et al., ACS Appl. Mater. Interfaces 11 (2019) 6881–6889.
[148] J.J. Kaczur, H. Yang, Z. Liu, et al., Front. Chem. 6 (2018) 263.
[149] M.A. Blommaert, R. Sharifian, N.U. Shah, et al., J. Mater. Chem. A Mater. 9 (2021) 11179–11186.
[150] J.C. Bui, I. Digdaya, C. Xiang, et al., ACS Appl. Mater. Interfaces 12 (2020) 52509–52526.
[151] S. Mafé, P. Ramírez, Acta Polym. 48 (1997) 234–250.
[152] K. Yang, M. Li, S. Subramanian, et al., ACS Energy Lett. 6 (2021) 4291–4298.
[153] K. Xie, R.K. Miao, A. Ozden, et al., Nat. Commun. 13 (2022) 3609.